energies

MDPI

Review

New Perspectives on Catalytic Hydrogen Production by the Reforming, Partial Oxidation and Decomposition of Methane and Biogas

Mattia Boscherini [1], Alba Storione [1], Matteo Minelli [1], Francesco Miccio [2,*] and Ferruccio Doghieri [1]

[1] Department of Civil, Chemical, Environmental and Materials Engineering, University of Bologna, 40126 Bologna, Italy
[2] Institute of Science, Technology and Sustainability for Ceramics, Italian National Research Council, via Granarolo 64, 84018 Faenza, Italy
* Correspondence: francesco.miccio@cnr.it; Tel.: +39-0547-699774

Abstract: The article provides a short review on catalyst-based processes for the production of hydrogen starting from methane, both of fossil origin and from sustainable processes. The three main paths of steam- and dry-reforming, partial oxidation and thermo-catalytic decomposition are briefly introduced and compared, above all with reference to the latest publications available and to new catalysts which obey the criteria of lower environmental impact and minimize the content of critical raw materials. The novel strategies based on chemical looping with CO_2 utilization, membrane separation, electrical-assisted (plasma and microwave) processes, multistage reactors and catalyst patterning are also illustrated as the most promising perspective for CH_4 reforming, especially on small and medium scale. Although these strategies should only be considered at a limited level of technological readiness, research on these topics, including catalyst development and process optimization, represents the crucial challenge for the scientific community.

Keywords: hydrogen; reforming; partial oxidation; autothermal reforming; dual/tri reforming; thermo-catalytic decomposition; catalysts; membrane

check for updates

Citation: Boscherini, M.; Storione, A.; Minelli, M.; Miccio, F.; Doghieri, F. New Perspectives on Catalytic Hydrogen Production by the Reforming, Partial Oxidation and Decomposition of Methane and Biogas. *Energies* **2023**, *16*, 6375. https://doi.org/10.3390/en16176375

Academic Editor: Alberto Abánades

Received: 31 July 2023
Revised: 27 August 2023
Accepted: 31 August 2023
Published: 2 September 2023

1. Introduction

Hydrogen and synthesis gas (syngas) are a fundamental intermediate for several key industrial processes, particularly ammonia and methanol synthesis as well as the Fischer–Tropsch process for production of synthetic fuels and oils and hydrogenation reactions of the petrochemical and chemical industry [1]. Furthermore, hydrogen is considered the leading candidate for substituting fossil fuels in power generation and storage (power-to-fuels approach), this transition representing a key strategy for the decarbonization of the energy industry to achieve the scenarios of carbon mitigation [2,3]. H_2-favorable energy-to-mass storage capacity and its completely CO_2 free combustion are the main advantages that today drive the increasing political and economic interest in its large-scale implementation in the energy field [4,5], while its high versatility and reactivity arouse interest in novel applications in the pharmaceutical, metallurgical and chemical industries [6]. As a result of the prospected growth of the world's energy and chemical demand, combined with the need to develop more sustainable processes with lower greenhouse gas emissions, hydrogen demand is predicted to increase dramatically in the near future, and new reliable and more sustainable pathways for its large and small-scale production are needed, with particular emphasis on production from renewable sources [7].

Hydrogen can be classified according to its material and energetic origin into grey hydrogen, black and brown hydrogen, blue hydrogen and green hydrogen [8]. Grey, black and brown hydrogen are produced from fossil sources, from natural gas (NG) reforming/partial oxidation, bituminous coal pyrolysis and lignite coal pyrolysis, respectively, with lowest

prices between 1.0 and 2.0 USD/kg, and nowadays it accounts for over 90% of the total global production of hydrogen, with large associated CO_2 emissions [9]. Blue hydrogen is also derived from fossil fuels, but with integration of carbon capture, storage and utilization pathways included in the production process to abate greenhouse gas emissions, and finally, green hydrogen is derived from water electrolysis powered by renewable sources. Another possible source for renewable hydrogen production is biomass, through either pyrolysis or gasification [10]. An illustration of hydrogen color according to production pathway is reported in Figure 1. It has to be noted that, while the classification of grey, brown, black and blue hydrogen is generally well defined [8,11–13], there is still debate on the color designation of other production sources. For example, the term yellow hydrogen, here designating hydrogen produced by power grid-riven electrolysis, as defined by Arcos and Santos [8], is sometimes used to designate instead hydrogen obtained from thermochemical solar splitting of water [11]. There is also not a general agreement on color classification of biomass-derived hydrogen, which is considered a green hydrogen production method by some authors when considering carbon neutral pathways [5,14] but a brown or blue hydrogen production method by others when considering non-renewable energy sources and the high CO_2 emission if carbon capture technology is not implemented [8].

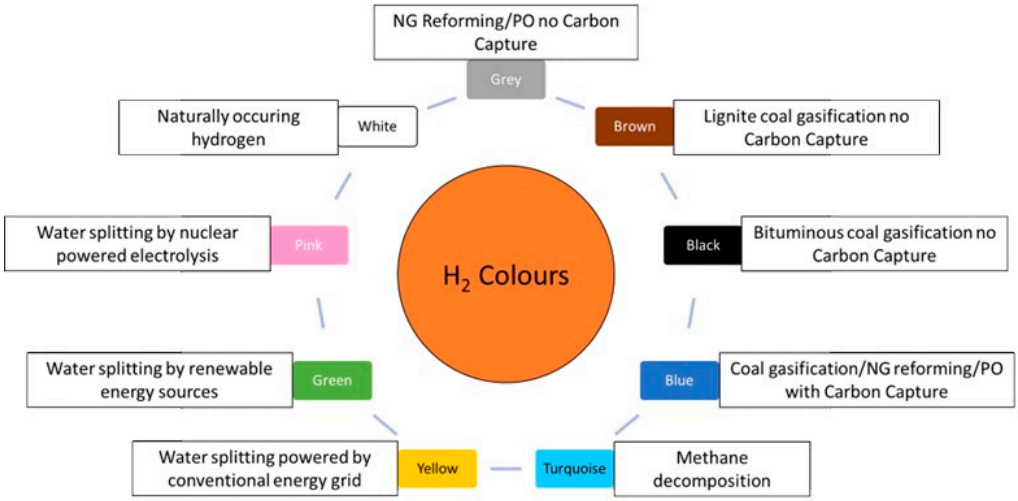

Figure 1. A common classification of hydrogen color according to production route.

Catalytic processes remain a crucial pathway for hydrogen production, especially for large-scale application, and much focus has been invested in research both for optimization of the current processes and the development of innovative and more sustainable pathways. Several reviews have been dedicated to H_2 production with thermochemical processes and related catalysts, dealing with both catalyst [15–18] and reactor/process design [19,20] and with different raw material for fuel [21–24]. It should be noted that while noble metal catalysts have repeatedly proved their high activity and stability for steam reforming [25], dry reforming [26] and partial oxidation [27] reactions, their high cost and scarcity renders their industrial application unfeasible, and therefore it was chosen to not include them in the present review. Several of these processes can also be potentially applied to biogas as well as natural gas, biogas being a complex mixture constituted mainly of methane and carbon dioxide derived from a variety of biological sources such as biomass waste material [28], which is particularly interesting from the perspective of green chemistry in order to lower carbon dioxide emissions and replace fossil fuels with new environmentally friendly alternatives; therefore, some applications of catalytic processes to biogas have also been considered, even though the presence of impurities such as sulfur compounds in biogas complicates its utilization compared to methane and natural gas [29,30].

The present article intends to review the current state of the art and future perspectives of catalytic hydrogen production from methane and biogas, mainly analyzing material

properties and process aspects aimed at improving productivity and yield for the product of interest. Thermochemical processes utilizing different feedstock, with particular focus on CO_2 reuse, and conventional and novel catalysts are analyzed, and their current advantages and limitations are critically discussed to put in evidence areas requiring further research. For details on the environmental and economic aspects of these processes, relevant considerations can be found in the following references [31–33], while more general reviews including also hydrogen transport, storage and utilization, as well as alternative hydrogen production sources such as water electrolysis, can be found in the following references [5,34–36]. This work presents itself as a continuation of reviews performed by Chen et al. [37] and Boretti et al. [38] by including the newest published results for catalyst development, with a secondary focus on process and reactor modeling and design. In particular, new perspectives on chemical looping, multistage processes, catalyst patterning and electrically assisted reforming are reviewed. For chemical looping processes, the promising application of cerium dioxide carriers is discussed.

2. Steam Reforming

Steam reforming of methane is the most common method for hydrogen and syngas production and it is responsible for the production of 47% of the global hydrogen [39,40]. A detailed review of the state-of-the-art reactor design for steam reforming reaction has been recently provided by Ganguli and Bhatt [20]. Most recently, a novel design for a composite scale microreactor was also presented, with potential for distributed production [41].

The main reaction for steam reforming of methane can be written as follows:

$$CH_4 + H_2O \longrightarrow CO + 3H_2 \Delta H^0_{298K} = +206 \frac{kJ}{mol} \quad (1)$$

Besides natural gas, heavy hydrocarbons and other feedstocks such as biogas can also be used. Typically, the process involves feeding methane and an excess of water vapor onto a Ni-based catalyst [42]. The process operates at a pressure between 3 and 25 bar, and the reaction is strongly endothermic; therefore, substantial heat has to be provided in order to maintain the process temperature at around 650–1100 °C [43]. This heat is usually provided by burning part of the hydrocarbon feed, but this approach is not environmentally friendly, as it leads to high carbon dioxide emissions [44]. The excess of feed vapor is required in order to avoid carbon deposition on the catalyst surface, but the need to produce large quantities of superheated vapor represents another large energy sink, limiting process efficiency and further contributing to high CO_2 emissions. Because of the high capital costs of equipment and its unsuitability, however, steam reforming technology is indicated for large-scale productions [45] (400 ton/d or above [46]), and is not suitable for medium- and small-scale plants (50 ton/d or below) [45], which would be needed to allow the distributed production of hydrogen.

As steam reforming is already a mature technology, at a TRL of 9 [9], current research is mainly focused on achieving further process optimization, by improving on current catalysts in order to increase process efficiency and reduce the problems correlated with carbon deposition [42], sintering [47] and catalyst poisoning [48] that limit the efficiency of conventional Ni-based catalysts. In particular, a Ni-based catalyst may be improved by providing adequate supports [49]. CeO_2 support, for example, has been investigated due to its potential for reducing coke deposition, thanks to its oxygen exchange properties [50]. The core-shell structure of the catalyst may provide a good solution for improving sintering resistance: for example, the core-shell of Ni/SiO_2 applied to both dry and steam reforming displayed no deactivation in 40 h during methane dry reforming, and only limited deactivation during the initial phase of steam reforming [51]. A porous yolk-shell-structured Ni/Al_2O_3 catalyst can offer good performance and improved resistance to alkali poisoning and carbon formation, improving its suitability for biogas reforming [52].

Bimetallic catalysts are another promising solution for steam reforming [53]. In particular, iron oxide can promote Ni activity and resistance to carbon deposition [54], allowing

for the reduction of the content of Ni and improving the lifetime of the catalyst. However, it is worth noting that Ni oxides are toxic and carcinogenic [55], and thus do not conform to green chemistry principles.

3. Dry Reforming

Due to the increased appeal of carbon capture technologies and decarbonization, interest in converting carbon dioxide to valuable products, such as syngas, methane and methanol, is becoming increasingly relevant in the chemical and energy industry [56]. Utilization of captured CO_2 as raw material for the production of intermediate chemicals is considered an interesting solution [57], as opposed to geological storage [58] and the application for further fossil fuel extraction through Enhanced Oil Recovery [59].

The dry reforming reaction (2) is considered a very interesting route for valorizing carbon dioxide by its conversion to synthesis gas through a reaction with methane, as it involves the simultaneous conversion of two common greenhouse gases and is particularly interesting for biogas conversion, as biogas is already a mixture of carbon dioxide and methane and can be treated without the need for an additional separation step [60–62].

$$CH_4 + CO_2 \longrightarrow 2CO + 2H_2 \Delta H^0_{298K} = +247 \frac{kJ}{mol} \quad (2)$$

The resulting produced syngas, with a H_2/CO ratio of 1, is particularly suitable for the synthesis of oxygenated compounds [63], but it can also alternatively be further processed in a water–gas shift unit, where carbon monoxide reacts with water, thus increasing the hydrogen production.

Dry reforming, on the other hand, is an even more endothermic reaction with respect to steam reforming, and the high operating temperature needed for the process (600–1000 °C [64]) represents a challenge in process design, particularly in avoiding catalyst deactivation by sintering. Carbon dioxide activation is very difficult, as it is a highly stable molecule [64]. Furthermore, the reaction is severely limited by high carbon deposition due to methane cracking (3) and the Boudouard reaction (4), which also causes rapid catalyst deactivation and parasitic reverse water–gas shift reactions between H_2 and CO_2 (5); this lowers the H_2/CO ratio of produced syngas below 1, making the produced syngas unsuitable for chemical synthesis and therefore lowering its economic value [49,65,66].

$$CH_4 \longrightarrow C + 2H_2 \Delta H^0_{298K} = 74.9 \frac{kJ}{mol} \quad (3)$$

$$CH_4 \longrightarrow C + 2H_2 \Delta H^0_{298K} = 74.9 \frac{kJ}{mol} \quad (4)$$

$$CO_2 + H_2 \longrightarrow CO + H_2O \Delta H^0_{298K} = 42.1 \frac{kJ}{mol} \quad (5)$$

Much work has been carried out on the development of catalysts for the dry reforming reaction, particularly to address the problem of deactivation due to coke deposition [67].

Ni-based catalysts are again the most common choice for the dry reforming reaction. Much interest is in the development of novel and optimized supports capable of limiting Ni sintering and carbon deposition, by evaluating new materials and more elaborated support structures. For example, Phan and Minh [68] investigated the use of wet precipitation-obtained calcium hydroxyapatite and Mg-doped calcium hydroxyapatite as support for wetness-impregnated Ni. They observed that catalytic activity and stability were affected by the Ca/P ratio of the support, with high ratios producing increased activity but reduced stability. They suggest the high activity of Ca-rich samples to be attributed to increased basicity and improved CO_2 adsorption. Mg addition showed no effect on activity, but it also improved stability. The maximum selectivity observed for syngas production was 85%, and all catalysts exhibited carbon deposition negatively affecting their

stability, while sintering appeared negligible. Nakajima et al. [69] investigated the kinetics of dry reforming on Ni-impregnated mesoporous MCM-41 silica support, and observed conversions higher than 85% at 973 K. They found that the reaction on their substrate could be described by the Langmuir–Hinshelwood mechanism. It should be noted that their investigated catalyst had a high Ni load, of 20%. Zhang et al. [70] also evaluated the effect of SiO_2 structure on the catalytic activity of Ni-impregnated catalysts and found that the best performance was obtained for monodispersed silica spheres (MSS) with inverted conical-shaped porosity at a 10% Ni loading. When compared to MCM-41 and commercial silica, MSS demonstrated improved pore impregnation and segregation of dispersed Ni nanoparticles that inhibited sintering and coking and reduced apparent activation energies for CH_4 and CO_2 decomposition, but the influence of reverse water–gas shift led to a final H_2/CO ratio slightly lower than 1. Similar results were obtained [71] for mesoporous SBA-15 silica and microporous beta silica: it was observed that, for catalysts prepared through the ammonia evaporation method for Ni deposition, beta silica had too small porosities, which did not allow proper Ni penetration, with the accumulation of Ni outside the pores leading to sintering and coking during the DRM reaction. The conventional impregnation method for Ni deposition also led to worse dispersion compared to the ammonia evaporation method [71].

The effect of Ni-support interactions for aluminum-nitride supports was inspected and it was observed that the formation of an ultrathin Al_2O_3 layer on the catalyst surface improved catalyst stability by preventing sintering and coking, achieving up to 89% conversion of methane with a 1% weight Ni load [72]. Haug et al. [73] investigated the effect of phase boundary structure for Ni/ZrO_2 catalysts. Interestingly, they found that an "inverted" catalyst, with a ZrO_2 phase deposited on the bulk Ni surface through chemical vapor deposition exhibited better anti-coking properties. Zhang and colleagues [74] analyzed the effect of a triple interface in $Ni\text{-}MgAlO_x/BN$ catalysts and found that a boron nitride surface successfully reduces coke formation by inhibiting the cleavage of the final C-H bond, while the $MgAlO_x$ surface acts as a dispersant for Ni particles inhibiting sintering and offers activation sites for CO_2, leading to stable 73.9% CH_4 conversion at 750 °C. Georgiadis et al. [75] investigated lanthanide oxides as support and found that while La oxides displayed the highest activity, they were also negatively affected by carbon deposition. Samarium oxide was suggested as the better option, as while slightly less active than lanthanum, it displayed significantly reduced carbon deposition. Cerium and praseodymium oxides, while coke resistant, displayed much lower activity, due to much weaker Ni-support interaction, and showed significant activity loss with time on stream.

Cobalt catalysts are also of interest for the dry reforming reaction. The addition of 10% yttrium promoter to the Co catalyst supported on WC-activated Carbon composite was shown to increase lattice oxygen availability, inhibiting coke formation while at the same time avoiding sintering and oxidation of Co particles [76]. Also, the proper selection of the calcination temperature (600 °C) increases catalyst stability, while yttrium addition inhibits the reverse water–gas shift reaction, ultimately improving the syngas H_2/CO ratio.

Depending on the preparation method, controlled adsorption or dry impregnation, cobalt-based catalysts supported on γAl_2O_3 bring about different performances. Indeed, the samples prepared by controlled adsorption displayed increased activity due to better Co dispersion and a lower tendency to deactivate for coke formation [77]. However, in both cases, coking led to catalyst deactivation within 8 h of reaction at 700 °C and the reverse water– gas shift reaction led to a H_2/CO ratio much lower than 1. Improved results were obtained for mesoporous Al_2O_3 support promoted with Y_2O_3 [78], for its use in optimized conditions; a methane conversion of 88.97% was recorded at 900 °C, with H_2 yield of 31.0% and CO yield of 69.4% (H_2/CO ratio ~ 1). Owgi et al. [79] compared the performance of Ni and Co catalysts supported on fibrous silica alumina and observed that Ni samples exhibited much higher activity and stability compared to Co, with a maximum conversion of CH4 of 97.5% for Ni/FSA and 20.6% for Co/FSA.

Ni-Co bimetallic catalysts show improved coke resistance when compared to monometallic Ni or Co catalysts; indeed, when the bimetallic alloy, Ni-Co, is supported on mullite, an increased activity and a better coke/sintering stability, compared to monometallic catalysts, can be achieved with more than 90% CH_4 conversion at 800 °C and showing only limited deactivation in 40 h on stream [80]. A 1:1 ratio of Ni:Co load was suggested as the optimal solution, as a catalyst with a higher Ni fraction displayed less activity, due to aggregation problems. Liang et al. [81] prepared Ni-Co nanoparticles encapsulated in attapulgite-derived MFI-zeolite and obtained a lower methane conversion of 71%, but their catalyst showed stable operation for 100 h. They propose that the zeolite shell not only confines metal nanoparticles avoiding sintering, but also helps in coke removal, thanks to its high sorption capacity for CO_2.

Copper and iron are cheap, non-toxic materials; therefore, their use in a catalyst is interesting from a safety and environmental point of view. The iron addition to a nickel-based catalyst supported on $MgAl_2O_4$ can bring the formation of a Ni-Fe alloy that reduces carbon deposition and increases CO_2 conversion, with the best Fe/Ni ratio equal to 0.7, as higher amounts of iron led to lower methane conversion [82]. Basicity of support also affects the performance of a catalyst, favoring CO_2 activation. Li et al. [83] also determined the best Fe/Ni ratio of 1 on Ce-Al_2O_3 at 600 °C. Higher-Ni-load catalysts would be more favorable for methane activation; however, they are prone to dealloying, leading to the formation of agglomerated Ni particles prone to deactivation by coking.

Ni/Cu supported on γAl_2O_3 in a ratio equal to 8:1 was found to be optimal for reaction at 650 °C. While limited deactivation and coking were still present for a bimetallic catalyst, it was seen that, for a Ni-Cu catalyst, mainly re-oxidable carbon was formed, compared to a monometallic Ni catalyst forming mainly refractory graphitic carbon [84]. The Cu presence partially suppressed the RWGS reaction, allowing for a stable 0.9 H_2/CO ratio. A Ni/Cu ratio of 8 was also confirmed as optimal by Han et al. [85] for catalysts on SiO_2 support, with stable 77.5% conversion of CH_4 and 84.5% conversion of CO_2. Khan et al. [86] developed and validated a Density Function Theory (DFT)-derived kinetic model for dry reforming on Ni-Cu catalysts. Such a modeling approach is able to provide an accurate description at the molecular level of the geometry, stability, and reactivity of chemical species adsorbed onto catalytic surfaces, and it is thus suitable for describing the reaction kinetics [87].

Other metallic pairs have been studied: a Co-Ce composite with a 3:1 Ce/Co ratio prepared through a glucose-assisted method displayed good activity (the maximum conversions of CH_4 and CO_2 were 87.2% and 54%) and stability, thanks to strong Ce-Co interactions [88]; Co-Sm, with yields of syngas >80% at 900 °C and no detectable carbon deposition [89,90]; and a Ni-Mo catalyst supported on monocrystalline MgO, a synthesized catalyst that offers high stability (850 h on stream) [91].

Perovskite-based catalysts are another alternative that is attracting much interest, thanks to the stability and tunability of the perovskite structure and reactivity by cation substitution. $LaFe_{0.9}Ni_{0.1}O_3$ perovskite displays improved performance when compared to Ni, Fe, and Ni-Fe La_2O_3-supported catalysts for dry reforming of ethane [92], thanks to the high dispersion of Ni nanoparticles formed in the reducing reaction environment and the fact that it remained stable over time, as well as the presence of oxygen vacancies that could dissociate CO_2. Suttiumporn et al. [93] investigated the effect of different M metal ions for $La_{0.8}Sr_{0.2}Ni_{0.8}M_{0.2}O_3$ perovskite, and found that while Cu substitution increased initial activity, Fe substitution allowed much higher stability. The stabilizing effect of Fe substitution was also confirmed for $La_{0.9}Sr_{0.1}NiO_3$ perovskite [94]: while the undoped perovskite irreversibly decomposed under DRM conditions, leading to increased coking, a 50% substitution of Ni by Fe permitted the obtaining of a more stable, regenerable perovskite structure with stable CO_2 and CH_4 conversion. Cerium doping in $La_{1-x}Ce_xNi_{0.5}Fe_{0.5}O_3$ enhances activity for dry reforming when x = 0.4–0.6, with high syngas selectivity [95]. More recently, a very stable (260 h on stream) Ni-Fe catalyst supported on $PrBaMn_{1.6}Ni_{0.3}Fe_{0.1}O_{5+\delta}$ double-layered perovskite has been obtained [96]. Remarkably, this latter material displayed promising stability and activity also for high pressure reactions.

4. Partial Oxidation

In a partial oxidation reaction, a hydrocarbon (typically methane) is reacted with sub stoichiometric oxygen to achieve its conversion to synthesis gas (CO + H_2) [97], as reported below for the case of methane:

$$CH_4 + \frac{1}{2}O_2 \longrightarrow CO + 2H_2 \qquad \Delta H^0_{298K} = -36\frac{kJ}{mol} \tag{6}$$

Contrary to steam reforming, partial oxidation is an exothermic reaction, avoiding the need to provide heat by combusting part of the hydrocarbon feed. While it is possible to operate with a purely thermal process, the use of a catalyst allows for a lower reaction temperature (800–900 °C for a catalytic process compared to 1200–1500 °C for a pure thermal process [98]). Partial oxidation also requires the supply of pure oxygen to avoid N_2 dilution of reaction products and has significant problems correlated with temperature run-off [99], which lead to loss in selectivity in favor of complete oxidation. As for dry reforming, coking [100], catalyst poisoning [101] and sintering [102] are also major issues for this process.

Ni-based catalysts have been vastly researched for PO on a variety of supports. Barbero et al. [103] investigated a Ni catalyst prepared by wet impregnation of La_2O_3, MgO and ZrO_2. La_2O_3-supported samples evolved into a perovskite structure and displayed the highest conversion, selectivity, and stability, while the ZrO_2-supported catalyst was the least active, and rapidly deactivated due to Ni sintering due to weak metal–support interaction. Good performance was obtained for 4% mol MgO-ZrO_2 support with 30% Ni load. In particular, higher MgO loading was found to increase coking, as the MgO-ZrO_2 solid solution formation was impaired [104]. Recently, Ni catalysts supported on fibrous and monolithic γAl_2O_3 have been compared, and the fibrous catalysts were found to achieve above 10 times the yield of their monolithic counterparts, thanks to better Ni dispersion and better mass transfer [105]. Fibrous catalysts also display high conversion and selectivity, with low carbon deposition, even for a high Ni loading of 45%, while the conventional wet-impregnated monolith sintered at high loading. Addition of magnesium to mesoporous alumina supports was investigated by Özdemir and Öksüzömer [106]: both Ni supported on MgO and Ni supported on $MgAl_2O_4$ displayed improved activity compared to the Al_2O_3 support. Interestingly, their samples were prepared through a solid combustion process without calcination. More recently, Khaleel et al. [107] determined that a 3% Fe doping of γAl_2O_3 support successfully reduces coke formation, and in particular the formation of crystalline carbon, without compromising activity.

MgO and MgAl mixed oxides have been evaluated as support also for Co-based catalysts [108]. While MgAl support displayed good activity, in this case samples supported on MgO experienced intense sintering and oxidation of Co species, leading to fast deactivation. An optimal 20 wt% Co load on 63 wt% MgO MgAl support was determined as the best-performing solution; however, carbon deposition was visible even for this catalyst. Choya and coworkers [109] instead evaluated the performance of Co supported on CeO_2/Al_2O_3 and found that a 12 wt% CeO_2 surface coating of alumina successfully weakened Co-Al_2O_3 interactions, inhibiting the formation of the inert cobalt aluminate phase, while increasing oxygen mobility. The resulting catalyst was, however, very sensitive to the presence of water in the reaction feed, which lead to partially irreversible deactivation. It has been previously observed that performance of a Co catalyst on γAl_2O_3 support prepared by chemical reduction could be increased by increasing the synthesis pH to 13.68 [110]. This latter catalyst displayed an initial methane conversion of 71.02% at 750 °C and a CO selectivity of 61.49% with a H_2/CO ratio of 2.05. Catalyst activity was stable for 70 h on stream, but after 110 h on stream the catalyst underwent a 27.15% loss in activity, due to coking.

Bimetallic catalysts have also been extensively studied for partial oxidation reactions. Fakeeha et al. [111] compared monometallic and bimetallic Ni and Co catalysts on ZrO_2-Al_2O_3 supports and determined that while monometallic catalyst performed best for a high calcination temperature, the Ni-Co catalyst provided the best conversion when the

calcination temperature was low. They attributed the negative effect of a high calcination temperature on the bimetallic catalyst to spinel phase formation. It should be noted that at 800 °C they observed selectivity of CO formation > 99% for all catalysts. Interestingly, they observed that the monometallic Co catalyst calcined at 800 °C provided the best activity and stability, outperforming both the monometallic Ni and bimetallic catalyst for this support. Cobalt addition was instead observed to be beneficial for the Ni catalyst on zeolite MCM-41 support [112], where formation of the Ni-Co alloy inhibited formation of NiO and prevented Ni atoms from destroying the molecular-sieve structure of the support. A 1% addition of Co offered the best performance, with stable 88% methane conversion for 100 h at 750 °C and GHSV = 18 L g^{-1} h^{-1} [113]. Synthetized Ni-Co catalysts supported on ZnO nanoprisms showed remarkable stability, with a methane conversion of 98.11% for 56 h on stream and a H_2/CO ratio of 2.11 [113].

The effect of Cu and Ce promoters for Ni catalysts supported on mesoporous silica SBA-16 was investigated too [114], and it was observed that while Ce addition provided a synergistic effect with Ni, resulting in high activity even for lower Ni loads, Cu addition was detrimental for catalytic performance [114]. Compared to the monometallic Ni catalyst, bimetallic Ni-Ce displayed the best activity for oxygen-rich feed, as the presence of Ce inhibited Ni oxidation. On the other hand, the H_2/CO ratio for these catalysts was consistently below the stoichiometric value of 2 and CO selectivity was low, which is attributed to the influence of the RWGS reaction and total combustion. Carbon formation was also present. This contrasts with previous research [115], where a high activity for a Ce-Cu catalyst prepared by the intermetallic route was observed, comparable to a noble metal catalyst. On the other hand, Ce-Cu catalysts obtained by the sol–gel method demonstrated much lower activity and poor selectivity. Ce addition was instead not beneficial on the SiO_2-supported Ni catalyst [116], displaying delayed methane activation, low conversion and high selectivity for total oxidation compared to monometallic Ni when the reaction was started at a low temperature and complete deactivating occurred after following the temperature ramp. The behavior of the cerium-doped catalyst was completely different when reaction was started above the methane reduction temperature, in which case Ni-Ce and Ni demonstrated similar behavior, with Ce not providing significant improvement apart from a slight enhancement in coke removal.

Perovskite catalysts have also attracted attention for PO. Loktev et al. [117] investigated $PrNi_{0.5}Co_{0.5}O_3$ and $SmCoO_3$ activity both for PO and DR reactions, and determined that while $PrNi_{0.5}Co_{0.5}O_3$ displayed high activity for DR but not for PO, $SmCoO_3$ instead exhibited high activity for both reactions, with syngas yield > 90% at 900 °C in both cases. The activity of samarium cobaltate for PO was recently confirmed [118]. Here, the surface modification through supercritical anti-solvent precipitation was found to provide higher coke resistance. $La_{1-x}Gd_xCrO_3$ with a varying Gd content (x = 0, 0.2, 0.5 and 0.8) was supported on porous Al_2O_3 [119] and tested in a burner reactor. All Gd-doped samples exhibited increased peak reaction temperature, compared to undoped samples, with increase in Gd doping leading to a reduction of the peak. The presence of the porous support successfully enhanced mass and heat transfer. The optimal yield for H_2 production was obtained for a Gd doping of x = 0.2 and a catalyst-support pellet size of 8 mm.

Molybdenum phosphide (MoP) was also evaluated as a catalyst both for the DR and the PO reaction [120], and it was found to exhibit different behavior. While for DR the catalyst displayed a methane conversion of only 65% at 900 °C and rapidly deactivated due to the coking formation of the Mo_2C phase and surface oxidation, a stable performance was obtained for the PO reaction, with near 90% methane conversion and 80% H_2 selectivity at the same temperature.

As the partial oxidation reaction is an exothermic and fast reaction, proper reactor design is essential to avoid formation of hot spots and to maintain a short residence time, to avoid complete combustion and excessive coking. While the non-catalytic partial oxidation process, despite still being less competitive than steam reforming, has already reached considerable maturity, particularly for higher hydrocarbon feedstocks (a novel

high-temperature reactor-design methodology was, for example, recently published and validated [121] for the partial oxidation of various hydrocarbon feedstocks), catalytic processes, while in theory allowing for a lower operation temperature, have so far only been demonstrated in pilot-scale plants; this is due to catalyst limitations [98], with only a few small-scale applications already commercially available [122], such as short-contact-time reactors [123].

5. Autothermal Dual/Tri-Reforming

As evidenced previously, steam- and dry-reforming reactions are highly endothermic, requiring considerable heat to be provided to the reformer reactor, while partial oxidation is an exothermic process which can be negatively affected by temperature runaway due to heat exchange impairments in the reactor. Furthermore, each process is only able to produce a syngas within a set range of H_2/CO ratio (maximum of one for dry reforming, two for partial oxidation and three for steam reforming), limiting the flexibility of the process and requiring further downstream treatments such as the water gas–shift reaction to tune the ratio to the desired value for further synthesis. These issues can both be addressed by combining the reforming and oxidation reactions in a single process. By properly tuning O_2/CH_4 and H_2O/CH_4 ratios in the feed stream, steam reforming and partial oxidation can be combined to obtain an autothermal steam-reforming (ATSR) process where the partial oxidation reaction provides the heat needed for the reforming without the need for external heat exchange [34]. Similarly, dry reforming and partial oxidation can also be combined in an autothermal dry-reforming process (ATDR) [124], while the steam-reforming and dry-reforming reaction can be combined in a dual-reforming process (2-R) to adjust the H_2/CO ratio (in this case, the process remains endothermic) [125]. The combination of all three reactions of SMR, DRM and PO, utilizing a combined $CH_4/CO_2/H_2O/O_2$ feed, is instead referred to as tri-reforming (TR) [126]. Both dual- and tri-reforming processes are particularly interesting for biogas, as well as, for flue gas conversion [62,127], as they avoid the need for separation of methane and CO_2 before reaction and, furthermore, the addition of water and oxygen to the reaction environment reduces the issue of carbon deposition that is predominant in pure dry reforming and allows good tuning of the H_2/CO ratio of produced syngas [14]. As previously seen for reforming and partial- oxidation reactions, catalyst design plays a crucial role also for coupled processes.

Ni-based catalysts are the most common choice for ATSR process [35,128], which typically operate in a temperature range of 800–1200 °C [129]. Support selection and preparation is crucial to ensure catalyst performance. For example, mesoporous γ-Al_2O_3 prepared by an easily scalable solid-state method was tested for autothermal reforming and displayed high surface area and methane conversion when calcined at 500 °C, with stable operation for 20 h on stream [130]. Further investigation by the same authors also investigated the effect of La_2O_3, CeO_2, ZrO_2 and SrO promoters on γ-Al_2O_3 catalysts and found that Ce promotion leads to the highest catalytic activity towards hydrogen production, as it also promotes WGS reaction [131]. Finally, a 3%-weight Ce addition was found to achieve optimal activity and resist carbon deposition [132]. Matus and colleagues investigated the effect of noble and non-noble metal promoters (M) on a Ni-M/$Ce_{0.5}Zr_{0.5}O_2/Al_2O_3$ catalyst and found that a Rhenium-promoted catalyst 10Ni-0.9Re/$Ce_{0.5}Zr_{0.5}O_2/Al_2O_3$ displayed self-activation capacity without the need for previous reduction, and stable reactivity with a high H_2 yield of 70%, close to that of a noble-metal-promoted catalyst [133]. Aurajo et al. [134] compared Ni catalysts supported on alumina and titanate perovskite and found that while all catalysts were active for the autothermal reforming, only perovskite-supported catalysts displayed stable operation, while alumina-supported catalysts deactivated due to sintering and nickel oxidation. Barium and calcium titanate displayed a high methane conversion of around 70%, while strontium titanate was much less active and exhibited coke formation due to weak metal–support interaction. Reactor design is particularly important for autothermal reformers and it has been the focus of substantial research. Considerable work has been dedicated to process optimization through numerical simulation, one of the most recent

examples being the work by Tariq et al. [135] for optimization of autothermal reforming on a NiO/Al_2O_3 catalyst through the response surface method. Their work evidenced that temperature is the most influential parameter for autothermal reforming, followed by steam-to-carbon and steam-to-oxygen ratio, and they obtained an optimal performance at 699.85 °C, 1 bar, steam-to-carbon ratio of 3 and oxygen-to-carbon ratio of 0.45. Murmura and colleagues [136] numerically compared three different reactor configurations: the conventional co-feed autothermal reformer, the spatially separated thermally coupled methane combustion and the reforming and distributed-oxygen-feed reformer. In the conventional reformer, oxygen is introduced to the reactor directly mixed with the methane and water feeds: this configuration allows for the reaching of equilibrium conversion in a very limited reactor space, but suffers from very high temperature peaks at the reactor inlet, which may negatively affect the catalyst and reactor durability and reduce process safety and controllability. On the other hand, the spatially separated configuration featuring a first catalytic combustion step thermally coupled to a consecutive reforming step and distributed-oxygen-feed configuration can obtain the same hydrogen yield as the conventional ATSR process at the cost of slightly larger reactors but avoiding dangerous temperature peaks. Folded reactors were also found to provide the opportunity for higher conversion and hydrogen yield in a numerical simulation by Chen and Wang [137] when compared to conventional and heat-pipe reactors. In particular, conventional tubular reactors suffer from heat exchange limitation that leads to inefficient heat transfer and poorer catalytic activity. In an alternative to conventional tubular reactors, a novel radial-flow spherical reactor was also recently proposed [138], minimizing CO_2 production and allowing higher flowrates and catalyst loading, thanks to a negligible pressure drop. Finally, Gul and colleagues [139] performed a numerical evaluation of a CO_2 sorption-enhanced autothermal dry-reforming process with CaO as CO_2 sorbent coupled with a Ni/MgO catalyst, allowing for a methane conversion as high as 94% with a 97% hydrogen purity.

Autothermal steam reforming has so far reached considerable technological maturity [14,122], and applications are already available on the pilot scale. The start-up and long-term operation of a 50 Nm^3/h pilot plant for biogas autothermal reforming has displayed high plant efficiency (68%) even for incomplete heat integration, without significative damage to the nickel catalyst employed during the start-up operation [140]. When operated with a noble-metal catalyst [141], the plant demonstrated flexible operation in a range of 20–100% of the design workload with a maximum plant efficiency of 75% and a production cost as low as 2.90 EUR/kg, which is advantageous compared to electrolysis and comparable to conventional SR. An economic analysis of biogas autothermal reforming for a 100 Nm^3/h plant also evidenced the possibility of reaching costs of hydrogen as low as 2.50 EUR/kg after 0 years' amortization [142].

Autothermal dry reforming has also recently received attention from researchers, particularly for biogas conversion, and a variety of catalysts and reactors have been investigated. Kelling et al. [143] proposed a multitubular ceramic counterflow reactor with easy scalability and increased capability of withstanding thermal stresses due to a high reaction temperature, but they used a noble-metal rhodium catalyst. Akri and colleagues prepared honeycomb monoliths of MgO-promoted Ni catalyst incorporated in illite clay and tested them for the reforming of a simulated biogas mixture [144]. The tested catalyst proved to be a cheap alternative to conventional wash-coated catalysts and displayed best performance for a 3% Mg loading and 8% Ni loading at 800 °C, with magnesium loading favoring Ni dispersion and preventing sintering. Nickel-upgraded slag oxide obtained from mining waste has been also positively investigated at 850 °C, obtaining a CH_4 conversion of 98% with 98.8% and 95.5% H_2 and CO yields and no observable loss of activity or coke deposition [145]. This catalyst was also found to be particularly resistant to hydrogen sulfide poisoning [146]. Rosha et al. [147] compared the catalytic performance of pure Ni nanoparticles in DR and ATDR and evidenced increased activity and lower carbon deposition (0.03% weight vs. 0.40% weight) in ATDR compared to DR. $CoAl_2O_4$-supported metal catalysts (Ni, Co, Rh and Ru) were tested in a cordierite monolith reactor [148].

The monolithic reactor performance compared favorably with the conventional Ni/Al_2O_3 fixed-bed reactor, with about 20% higher reaction rates and up to 40% higher methane conversion at the high flowrate, thanks to better distribution and greater availability of metal active sites due to the increased surface area of monoliths. Of the metal species investigated, rhodium displayed the highest catalytic activity, followed by nickel. As one of the limitations of ATDR is that addition of O_2 to the reaction mixture can lower CO_2 conversion, dual-site catalysts capable of improving CO_2 activation are of interest for the dry-reforming reaction: for example, addition of CeO_2 and ZrO_2 to a SiO_2 support for Ni catalysts was observed to remarkably include catalytic performance, providing CO_2 conversion close to the equilibrium value in a temperature range of 600–800 °C [149]. More recently, the effect of the addition of CeO_2 and ZrO_2 promoters to the alumina support for the Ni catalyst was also investigated, with cerium dioxide performing the best in terms of performance improvement [150]. Setting themselves apart from conventional thermochemical process, Fan et al. [151] proposed instead an innovative design for a novel Solid Oxide Fuel Cell reactor for the cogeneration of syngas and electrical power through ATDR. This process may be particularly advantageous, in that it does not require oxygen purification and avoids forming potentially dangerous CH_4/O_2 mixtures. The researchers demonstrated a stable operation for 120 h at 800 °C, with a hydrogen selectivity of 80% and stable 65% methane conversion.

Nickel-based catalysts are also the most common choice for the dual-reforming of methane [152], and have been recently reviewed [153,154]. Most recently, Jin et al. [155] demonstrated significantly improved catalytic performance of a non-stoichiometric cerium oxide-overcoated Ni/Al_2O_3 catalyst prepared through atomic layer deposition compared to an uncoated catalyst, with an increase in reaction for methane conversion from 61.9% for the uncoated catalyst to 87.2% for the coated sample at 800 °C. A bimetallic Ni-Co catalyst supported on cerium dioxide- and magnesia-promoted alumina was found to exhibit stable operation for 500 h with negligible carbon formation, 97% methane conversion and 89% CO_2 conversion at 850 °C [156]. As the 2-R process is highly endothermic, solar energy is potentially a green alternative for providing the required reaction heat: Storch et al. [157], however, evaluated that dual reforming of methane can only be effectively applied for a CO_2/CH_4 ratio up to 0.35. Thermodynamic analysis determined that for dual reforming optimal reaction conditions require atmospheric pressure, temperature above 800 °C, oxygen-to-carbon ratio greater than 1.1 and a carbon dioxide-to-steam ratio of 1.5–2 [158].

Catalysts for the methane tri-reforming process are also prevalently nickel-based [159,160], and a recent review on thermodynamic evaluation, operation conditions and reactor configuration has been provided by Soleimani and colleagues [161]. Kozonoe et al. [162] compared carbon nanotubes and silica support for Ni catalysts and found that while both supports showed stable activity, carbon nanotubes offered better methane and carbon dioxide conversions, and also greater selectivity for hydrogen formation at 750 °C, mainly attributed to lower carbon dioxide activation by silica due to the acidic nature of the support. The deactivation behavior of bimetallic molybdenum catalysts supported on lanthana-alumina and on niobia determined that only NiMo catalysts are active on a lanthana-alumina support, while PtMo is active on a niobia support [163]. On a lanthana-alumina support, the Pt bimetallic catalyst rapidly deactivated due to sintering, while the CoMo catalyst deactivated due to oxidation of the cobalt species both on the lanthana-alumina and the niobia support. The nickel bimetallic catalyst on the niobia support instead deactivated due to intense carbon deposition. It should be noted that while lanthana addition to the alumina support for nickel catalysts initially increases hydrogen yield, an excess of lanthana causes increased carbon deposition due to the formation of an inactive $LaAlO_3$ phase [164]. A study of catalytic activity of $LaNiO_3$ perovskite with partial Ni substitution by Ce or Sr dopants demonstrated that conversion of methane was similar in undoped and doped samples (75%) but the cerium-substituted catalyst displayed greater CO_2 conversion and lower hydrogen selectivity due to higher CO formation [165]. This can be attributed to the improved activation of carbon dioxide due to improved oxygen

exchange by the Ce^{3+}/Ce^{4+} easy interconversion. At the time of this review, reactor studies for the tri-reforming process are mostly theoretical. Jang and Han [166] proposed that a distributed feed of oxygen to the reformer reactor can offer better process control and flexibility by achieving better control of the temperature profile and reducing mass and heat-exchange limitations. Aboosadi et al. [167] produced a model for a slurry bubble column reactor with a NiO-Mg/Ce-ZrO_2/Al_2O_3 catalyst and obtained a 92% methane conversion with a 1.76 H_2-to-CO ratio in optimized conditions. The main advantage of the slurry bubble column reactor is the prevention of hot spot formation. A 2-D axisymmetric model was produced for estimating process optimization of a fixed-bed reactor for different final objectives: maximization of H_2/CO ratio and energetic efficiency (case 1), maximization of H_2/CO ratio and carbon dioxide conversion (case 2), and maximization of carbon dioxide conversion and energy efficiency (case 3) [168]. The decision variables selected were inlet temperature, oxygen–methane ratio and carbon dioxide–methane ratio. For case 1 the scenario requires an increase in the oxygen inlet, a decrease in the carbon dioxide fraction and a reduced inlet temperature. At optimized conditions, methane conversion reaches 60%, but carbon dioxide conversion is below 10%. For case 2, maximizing carbon dioxide conversion requires increasing the inlet temperature to favor the dry-reforming reaction and inhibit the water–gas shift, while also lowering the oxygen content in the feed. An increase in carbon dioxide conversion inevitably leads to the lowering of the hydrogen-to-carbon monoxide ratio, as more CO is produced. For case 3, if a compromise of 1% is accepted for the requirement for energetic efficiency, a carbon dioxide conversion of 26.2% and a methane conversion of 80% can be achieved with a H_2/CO ratio of 1.5. Finally, the substitution of conventional steam reforming with tri-reforming for syngas production in methanol synthesis was evaluated and it was concluded that improved methane conversion and reduced carbon dioxide emissions can be obtained with this approach [169].

In contrast with autothermal steam reforming, ATDR, 2-R and TR processes are still in the early stages of development and have not been applied yet on a commercial scale.

6. Thermo-Catalytic Decomposition

While for the steam/dry reforming and partial-oxidation reaction coke formation is an undesired parasitic reaction, the direct decomposition of methane (3) is another possible pathway for producing hydrogen and carbon. In fact, because of inert conditions, no carbon oxides are expected to be formed.

Reaction (3) is thermodynamically favored at a high temperature (>1300 °C) and low pressure (atmospheric) [170]. Thermo-catalytic decomposition (TCD) in the presence of suitable catalysts allows the process to be carried out at lower temperatures of 500 to 1000 °C [170,171] but with more limited CH_4 conversion, because of thermodynamic limits.

Methane TCD has been recently reviewed [172,173], also addressing catalytic solar-assisted decomposition, as well as the innovative CH_4 cracking in molten salts (e.g., NaCl, NaBr, Na_2CO_3-KCO_3, KCl-$NiCl_2$, and $MnCl_2$-KCl) [174–176].

As far as catalysts are concerned, metals like Ni, Co and Fe are active for lowering the process temperature down to 600 °C, but the deactivation by carbon deposition is even larger as the temperature decreases. Iron seems to be more resistant to deactivation, as well as the support playing a relevant role, with good interaction and dispersion of the metal particles on the support preventing the agglomeration and the sintering of the catalyst. Msheik et al. [172] also reviewed the use of carbonaceous catalysts (chars of various origins) that, despite lower effectiveness than metals, boast several advantages, such as lower cost, resistance to high temperature, safe storage, tolerance to impurities such as sulfur, no contamination of the carbon byproduct, generally no need for regeneration, additional self-catalysis, and mitigation of CO_2 emissions.

The influence of the addition of various transition metals (Cu, Cr, Co, Zn, and Mn) on the properties and efficiency of the NiO(50)/$FeAl_2O_4$ catalyst was investigated in a micro fixed-ed reactor [177]. The Mn-based catalyst was the most effective among others

in terms of catalytic activity and stability, with production of high-purity hydrogen and nanostructured carbon particles, at a temperature of 700 °C with CH_4 conversion of 62.3%.

Owing to the allo-thermal character of TCD, fluidized bed technology was proposed and applied, thanks to the high heat-transfer coefficient, of up to 300 W $m^{-2}K^{-1}$ [178]. Ni-Cu-Al oxide systems were synthesized and tested in an FB reactor for the methane decomposition yielding H_2 and carbon fibers, with methane conversion of 40% at 675 °C [179]. Ammendola et al. [180] developed different CuO/Al_2O_3 catalysts by co-precipitation and wet impregnation of supporting granules (300–400 μm), for fluidized-bed operation. The active phase and the best catalyst superficial catalyst composition was determined by TPR analysis, reporting an optimal composition for a copper–aluminum spinel. The applicability of catalysts in a bench-scale fluidized bed was investigated at 800 °C. The catalyst was in the class B of Geldart classification [181], thus well-suited for fluidization, and characterized by a limited attrition rate, i.e., 3.0×10^{-5} %/min. A two-stage operation for H_2 production in FB was investigated [182], consisting of first operating TCD until a defined catalyst deactivation degree is approached, and then operating the fluidized bed as a combustor or a gasifier for catalyst regeneration by carbon removal. Three different strategies of catalyst regeneration, by air, CO_2 and steam have been assessed, along with the optimization of the times for decomposition and regeneration steps. The authors concluded that regeneration time, preferably conducted in air for kinetic reasons, is a compromise between reducing catalyst re-oxidation and removing large amounts of deposited carbon.

7. Discussion

Table 1 reports the classification of the reviewed articles. Critical raw materials (CRM) rely on the recent European Commission Communication of 2023 [183], including 34 elements. CRMs have been selected when an element reaches or exceeds the thresholds for both economic importance and supply risk for European countries, the threshold for supply risk being lower than that for economic importance. The harmfulness is instead based on the safety-data sheets of the individual compounds.

Table 1. Classification of reviewed articles.

Process	Technology Readiness	Catalysts	CRM	Harmfulness	Refs.
Steam reforming	Commercial	Ni	N	Y	[39–41]
		Ni-Fe	N	Y	[53]
Dry reforming	Lab scale	Ni	N	Y	[58–64]
		Co	Y	Y	[65–68]
		Ni-Co	Y	Y	[69,70]
		Ni-Cu	N	Y	[73–75]
		Ni-Fe	N	Y	[71,72]
		Co-Ce	Y	Y	[88]
		Co-Sm	Y	Y	[89,90]
		Ni-Mo	Y	Y	[91]
		Perovskite *	Y	Y-N	[80–84]
Partial oxidation	Pilot–Commercial Lab scale	Ni	N	Y	[91–95]
		Co	Y	Y	[96–98]
		Ni-Co	Y	Y	[99,113]
		Ni-Cu	Y	Y	[102,103]
		Ni-Ce	Y	Y	[102,104]
		Cu-Ce	Y	N	[115]
		Perovskite *	Y	Y-N	[105–119]
		MoP	Y	N	[120]
Thermo-catalytic decomposition	Lab scale	Ni-Mn	Y	Y	[177]
		Ni-Cu-Al	Y	Y	[179]
		Cu	Y	N	[180]

* Variable structure.

Overall, the level of technological readiness is advanced for steam reforming and good for partial oxidation, whilst the other two processes (DR and TCD) are still to be implemented at an industrial level. The studies of the catalysts mainly concern laboratory characterization of the developed materials, which are often tested with very small-scale instrumentation (TGA, TPR, etc.) and for limited catalyst time on stream (no more than 200 h). So far, the optimization of catalysts and supports has provided many novel solutions, but the issue of ensuring a good compromise between catalyst lifetime and activity has yet to be solved. Table 2 reports the main advantages and disadvantages of each catalytic process, while Table 3 summarizes operation conditions, process efficiency and hydrogen production cost.

Table 2. Main advantages and disadvantages of methane-conversion technologies.

Process	Advantages	Disadvantages	Refs.
SR	High H_2/CO ratio (=3) Mature technology	Excess high-pressure steam needed (steam/C: 2–5; 3) Endothermic reaction High CO_2 emission High capital costs	[49–53]
DR	CO_2 utilization Applicable to biogas without previous separation	Low H_2/CO ratio (=1) RWGS parasitic reaction can decrease the syngas ratio below 1 Strong tendency for carbon deposition Endothermic reaction High reaction temperature needed (risk of catalyst sintering)	[68–86,88–96]
PO	Exothermic process More compact reactors, thanks to fast kinetics Moderate syngas H_2/CO ratio (=2) Non-catalytic operation is possible	Pure O2 is needed (expensive ASU unit) Difficult temperature and selectivity control Risk of explosion (CH_4-O_2 mixture) Coking can deactivate catalyst	[103–120]
ATSR	Mature technology Compact reactors Increased energy efficiency Reduced capital costs compared to SR Lower steam and oxygen requirements compared to SR and PO Lower operating cost compared to SR	Pure O_2 needed Risk of explosion (CH_4-O_2 mixture) Coking and sintering can deactivate catalyst Low H_2 yield compared to SR	[130–135]
ATDR	CO_2 utilization Applicable to biogas without prior separation Autothermal process Lower oxygen and no steam requirement	Pure O_2 needed Risk of explosion (CH_4-O_2 mixture) Coking and sintering can deactivate catalyst	[144–150]
2-R	CO_2 utilization Applicable to biogas without prior separation Tunable H_2/CO ratio Lower carbon deposition compared to pure SR and DR	Strongly endothermic process Coking and sintering can deactivate catalyst	[152–156]
TR	CO_2 utilization Applicable to biogas without prior separation Tunable H_2/CO ratio Presence of oxygen lowers endothermicity Lower carbon deposition compared to pure SR, DR and PO	Pure O_2 needed Risk of explosion (CH_4-O_2 mixture) Coking and sintering can deactivate catalyst Difficult management of competitive oxidation–reforming reaction	[159,160,162,163,165]
TCD	Zero or near-zero carbon dioxide emission (no CO_2 formation) Highest yield of hydrogen (no CO formation) Less complex separation of produced hydrogen (easy separation from solid carbon) Carbon can be produced in value-added form (nanotubes, nanosheets, etc.) No oxygen or steam requirement	Endothermic reaction Coke formation leads to difficult continuous operation due to catalyst deactivation and reactor clogging Harsh reaction conditions cause problems for durability of reactor materials	[177,179,180]

Table 3. Literature data for process efficiency, operation conditions (T and P) and H_2-production cost for catalytic hydrogen production from methane. (CCS is short for Carbon Capture and Storage, technologies for CO_2 emission abatement [184], N.A. indicates data that were not available in the literature).

Process	Efficiency (%)	T (°C)	P (Bar)	H_2 Cost
SR	70–85 (no CCS) [5,9,14,35,124] 60 (with CCS) [185]	650–1100 [44]	3–25 [44]	0.9–1.8 USD/Kg [14] 2.08 USD/Kg (no CCS)–2.27 USD/Kg (with CCS) [34] 1.83–2.35 USD/Kg [35] 1.54–2.30 USD/Kg [9]
DR	76 (estimated for biogas reforming) [186] 59 (estimated for power and H_2 cogeneration) [187]	600–1000 [53]	N.A.	0.15 EUR/Nm^3 (power and H_2 co-generation) [187] 2.38–3.27 USD/Kg (coke-oven-gas reforming) [188] 1.07–1.32 USD/Kg (no CCS)—1.91 USD/kg (with CCS) [189]
PO	N.A.*	800–900 [100]	N.A. *	N.A.
ATSR	90 [14] 60–75 [190]	800–1200 [131]	1–30 [131]	1.48 USD/Kg (with CCS) [34]
ATDR	N.A.	N.A.	N.A.	N.A.
2-R	82 (natural and biogas co-reforming) [188]	N.A.	N.A.	N.A.
TR	N.A.	N.A.	N.A.	N.A.
TCD	58 [187,191]	500–1000 [162,163]	1 [162]	2 USD/Kg [8] 2.55–5 USD/Kg [12] 3.53–3.82 USD/kg [192] 1.72 USD/kg

* Data available in literature refer to non-catalytic process.

As far as issues of economic and environmental impact are concerned, almost all the elements used belong to the CRM category, except for Ni, which, however, is considered harmful. Iron, manganese, and copper should be considered of great relevance for future application, both being easily available also from waste recycling.

8. Novel Perspectives

8.1. Chemical Looping

In recent years, a lot of attention has been given to the study of transport properties of solid compounds, the chemical looping technologies and their mutual integration, to overcome the limits of traditional processes [193].

In a looping configuration the reaction scheme can be split into two separate steps. allowing for a higher flexibility with respect to that achievable in the traditional processes. Figure 2 provides some examples of typical looping configurations [194].

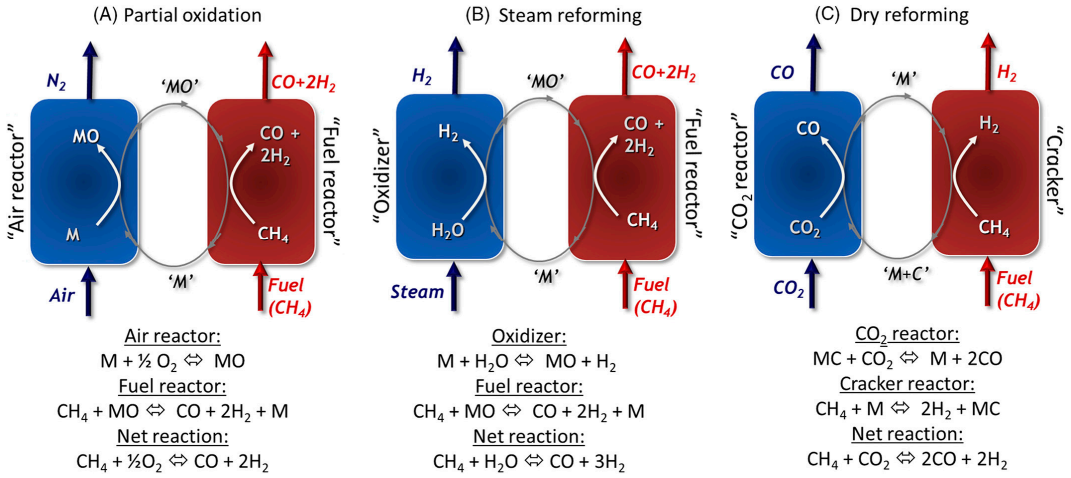

Figure 2. Looping configuration for hydrogen and syngas production.

In a looping process, in the first step the fuel (methane in the reported example) is selectively oxidized to syngas or hydrogen (7), while in the second step the OC is re-oxidized through reaction with H_2O (8), CO_2 (9) or oxygen/air (10).

Step 1

$$\delta CH_4 + MeO_x \longrightarrow \delta CO + 2\delta H_2 + MeO_{x-\delta} \quad (7)$$

Step 2

$$MeO_{x-\delta} + \delta H_2O \longrightarrow 2\delta H_2 + MeO_x \quad (8)$$

$$MeO_{x-\delta} + \delta CO_2 \longrightarrow \delta CO + MeO_x \quad (9)$$

$$MeO_{x-\delta} + \frac{\delta}{2}O_2 \longrightarrow MeO_x \quad (10)$$

The chemical looping operation can be achieved either in a continuous circulating fluidized-bed configuration or through a semi-continuous process where the looping is achieved by the switching of the gaseous atmosphere over a fixed or fluidized bed [195]. In all cases, the product streams are inherently separated, allowing greater process flexibility, as the CO stream produced in oxidation can be either used alone or mixed with the stream of syngas produced during reduction to correct the H_2/CO ratio.

The use of a looping configuration also allows for the decrease in the likelihood of undesired reactions. An example of this can be provided by the chemical looping dry reforming of methane (CL-DRM). Here, the use of the carrier for the transfer of oxygen allows the avoidance of the effect of the reverse water–gas shift reaction, as the reactant CO_2 and the product H_2 do not come in direct contact. CL is also beneficial for partial oxidation, as the inherent separation between reactants reduces the risks of explosion and removes the need of an air-separation unit to produce pure oxygen (Figure 2A).

Among a variety of options, thermochemical water splitting brings high conversion of hydrogen at high purity and if it is practiced in association with the utilization of a fuel (steam-reforming process), the temperature and energy demand considerably decrease, thanks to the enhanced reactivity of the oxygen carrier in presence of a reducing agent (Figure 2B). In this respect, selection of proper oxygen carrier material is essential for chemical looping applications: key parameters for an oxygen carrier are fast redox kinetics, high oxygen-storage capacity, resistance to sintering and carbon deposition, and thermal and mechanical stability (for fluidized- and circulating-bed applications) of the structure over repeated cycles [196]. Several different materials have been evaluated for CL-DRM: iron-based OCs have the advantages of relatively low costs and environmental safety and they can be successfully re-oxidized by carbon dioxide displaying high oxygen-storage

capacity, but they tend to suffer from severe sintering problems and generally slow reaction kinetics with methane [193,197]; Chuayboon et al. [198] tested the performance of an iron oxide OC during a methane reforming–water splitting process heated by solar radiation, and found that the material performance depended strongly on temperature and degraded rapidly over only five cycles. As CO_2 is a much weaker oxidant compared to water, these limitations would presumably become more pronounced for a CL-DRM process. On the other hand, Ni-based oxygen carriers display high methane conversion, but they suffer from high carbon deposition, higher costs, and toxicity, and cannot be re-oxidized directly by CO_2 [67,193,199]. Mixed Ni-Fe materials have also been investigated [197,200], in an attempt to combine the properties of both metals to overcome their respective limitations, and perovskite oxides have also received attention [201].

Noble-metal catalysts (Rh, Ru, Pd, Pt, and Ir) show high catalytic activity and stability for dry reforming, with scarce carbon deposition, but they can hardly find large-scale application, due to their high price. On the contrary, transition metals such as Ni-, Co-, Cu-, Mn-, and Fe-based catalysts, are highly promising, due to their abundance, low cost, and good thermodynamic properties for reforming processes [202–204].

Solid transition-metal (Ni, Co, Fe, Cu)-based catalysts interact with hydrocarbons, breaking the C-H bond and favoring the decomposition at a lower temperature, being suitable for the direct production of hydrogen if mixed in alloy and applied molten [46] (Figure 2C). In this case, the material acts as carbon carrier and pure streams of H_2 and CO are produced [205].

Cu-based oxygen carriers show suitable redox behavior to ensure a good oxygen transfer capacity, along with good reactivity for the reforming reaction. They are also capable of directly releasing oxygen by thermal decomposition at medium-high temperatures (800–1000 °C) [206]. Also in favor of these systems is their low price and limited toxicity, but they can give rise to sintering and melting even at temperatures below 800 °C and be subjected to friction, due to limited mechanical strength. These limitations are partially overcome by employing support, for example, with γ-Al_2O_3, MgO, SiO_2, CeO_2, and ZrO_2, or promoters such as alkaline and alkaline earth metals, as well as rare earth metals, which remarkably improve catalytic performance and reduce coke formation, especially in the dry-reforming processes.

Among the various available oxygen carrier materials, cerium dioxide (CeO_2) shows some of the most promising properties for methane-reforming processes, both as support for Fe [207,208], Ni [203,209] or Co [204] or applied individually without inclusion of supports; therefore, its use has been analyzed in more detail in this review.

Cerium dioxide, despite being a lanthanide oxide, is rather abundant in the Earth's crust, being comparable to copper [210]. The use of CeO_2 as an oxygen carrier for methane reforming was first proposed by Otsuka et al. [211], who studied the behavior of this oxygen carrier in a temperature range between 570 and 750 °C. They demonstrated that cerium dioxide could selectively produce syngas with a H_2/CO ratio of 2, with limited production of water and CO_2 at the beginning of the reduction step, and that CO_2 can be used effectively for regeneration. Cerium dioxide, in fact, displays very high oxygen-storage capacities associated with the Ce^{4+}/Ce^{3+} redox pair, its reduction leading to the formation of a continuous range of non-stoichiometric species ($CeO_{2-}x$, with $0 < x \leq 0.5$) that nonetheless preserve the original cubic fluorite structure [212,213]. Thermal stability of cerium dioxide may be improved by doping with tetravalent ions, for example Zr^{4+}, which also has the advantage of improving oxygen storage and exchange by facilitating the migration of bulk oxygen species during reduction [213,214].

CeO_2 reduction and oxidation are easily reversible [215–217] and the material also displays fast internal oxygen diffusion [218] and high resistance to coke formation, being able to catalyze the combustion of deposited carbon [219,220].

Temperature-programmed reduction experiments with methane as the reducing agent [216,220–222] show that cerium dioxide is active for methane partial oxidation at temperatures above 700 °C, and the selectivity towards partial oxidation is high, with

limited total oxidation of methane occurring at the beginning of reduction when more surface oxygen species are available. A limited influence of the methane cracking reaction was observed in all the examined studies, occurring once a high oxygen depletion of ceria was reached.

Chuayboon et al. [198] compared its performance with that achievable by employing iron oxides for methane reforming coupled with water splitting. The CeO_2 carrier was found to provide improved performances compared to iron oxides in terms of reactivity and stability over repeated cycles. Stable operation was also observed for 10 cycles at T = 1000 °C with stable syngas yield (5.67–6.80 $\frac{mmol}{g_{CeO_2}}$) and selectivity (96.5–98.2%) and a notable methane conversion (46.9–60.9%).

Methane reforming in looping, in presence of cerium dioxide, has been carried out employing solar reactors as a source of heat [192,200,201]. Nair and Abanades [214] tested the performances of three different cerium dioxide structures, consisting of unmodified commercial cerium powder, ceria prepared through a hydrothermal templating method and ceria prepared through a self-assembly method over two/three isothermal reduction/oxidation cycles at 1000 °C. TGA experiments on these materials revealed that all of them could be almost completely re-oxidized by CO_2, but unmodified commercial dioxide showed structural instability, demonstrating rapid sintering and a decrease in CO yield during CO_2 splitting (from 0.365 $\frac{mol_{CO}}{mol_{CeO_2}}$ for the first cycle to 0.322 $\frac{mol_{CO}}{mol_{CeO_2}}$ for the second cycle). The self-assembled and hydrothermally prepared samples overall displayed more stable performances (with CO yields of 0.360–0374 $\frac{mol_{CO}}{mol_{CeO_2}}$ and 0.341–0.347 $\frac{mol_{CO}}{mol_{CeO_2}}$ respectively), while also displaying overall faster kinetics. Oxidation with carbon dioxide, as expected, was found to be slower than oxidation with water.

Warren et al. [223] instead investigated the performance of commercial CeO_2 powder, evaluating the effect of different operating conditions: temperature, flow rates and initial extent of CeO_2 oxygen non-stoichiometry. Interestingly, they observed that starting the reduction phase over oxygen-deficient cerium dioxide leads to higher selectivity toward syngas formation, lowering CO_2, H_2O and coke formation. It also allows for the achievement of faster oxidation during the regeneration phase with CO_2. A performance over 10 redox cycles at 1170 °C with a 4 min reduction time and 2 min oxidation resulted in a stable performance of the material, with a significant averaged conversion of reactants (69% for CH_4, and of 88% for CO_2), and a high selectivity towards H_2 and CO (99% and 93%, respectively). Also, carbon formation was found to be absent after a proper selection of the reaction time.

Finally, Chuayboon et al. [224] compared commercial cerium powder with structured porous foams and mixed powders of CeO_2 and Al_2O_3. Oxidation with CO_2 was performed for CeO_2 and Al_2O_3 mixed powders at different temperatures (950–1050 °C), confirming the increase in syngas yield and reaction kinetics during reforming with increasing temperature. Temperature was found to have no relevant effect on oxidation. Overall maximum yields of H_2 and CO were found to be of 5.11 and 5.04 $\frac{mmol}{g_{CeO_2}}$ at 1050 °C, also considering methane cracking and coke combustion side reactions. The shape of the material was found to have no relevant impact on syngas yield, as CeO_2 powder and foams showed no relevant differences.

The thermodynamics of this reforming process was also investigated [225], and it was demonstrated that cerium dioxide can be efficiently used for isothermal operation at a temperature of 950 °C. The need for reaction temperatures above 900 °C was also determined [226], utilizing ASPEN Plus as a software simulator for thermodynamic predictions.

The mechanism of reaction of CeO_2 with methane and carbon dioxide was investigated by Warren and Scheffe [227], who found that partial oxidation of methane over cerium oxide follows different reaction mechanisms according to the degree of reduction and to the presence of oxygen vacancies in the structure of the material, with different kinetic limitations for low- or high-oxygen-depleted ceria. Interestingly, they found that hydrogen presence inhibited the reaction rate during reduction only for high-oxygen non-

stoichiometries cerium dioxide, and that reaction rates seem not to be limited by bulk diffusion [114]. Both higher temperatures and higher methane partial pressure were found to increase reaction kinetics.

The kinetics of cerium dioxide oxidation with CO_2 were instead studied by Ackermann et al. [228], who found that the rate of reaction is suppressed for high-oxygen non-stoichiometries in a temperature range between 420 and 1000 °C. Welte et al. [229] performed an interesting study of CeO_2 reduction in a moving-bed particle reactor. They observed that a co-current flow of CH_4 and CeO_2 is needed to avoid further oxidation of syngas with cerium dioxide, which may also be possible near the exit of fixed-bed reactors where the methane concentration is lower than syngas. They also observed that carbon formation was suppressed at temperatures above 1300 °C.

In conclusion, this technique represents an interesting possibility for carrying out processes that require the supply of an oxidizing reagent without contamination with inert species (e.g., N_2), especially if conducted on a limited scale, for example, such as those situations in which the use of oxygen from air distillation is not economically convenient.

8.2. Electrically Asssited Reforming

Recently, the application of an electrical current/field to chemical reactors has attracted considerable interest, at least for lab-scale investigations. Compared to conventional purely thermo-catalytical processes, these techniques (e.g., microwaves, hot/cold plasma) enhance the performance of the reforming process allowing for catalyst activity at a reduced temperature.

The effect of support structure on Ni/γAl_2O_3 catalysts in plasma-assisted catalytic reforming was evaluated [209] and it was concluded that Al_2O_3 nanosheets are the best support compared to nanorods or spherical flowers, displaying smaller and better-dispersed Ni particles and achieving the best plasma–catalyst synergy. thanks to the high number of exposed Ni sites, improving charge transfer [230]. Higher than 90% methane conversion without external heating was achieved in their experiment.

Microwave (MW)-assisted methane DR was investigated [231] in a custom-designed reactor housed inside an MW apparatus. The authors reported the advantage of process intensification and reaction stability in their process compared to the conventional heated reactor, probably for the generation of local hotspots (micro-plasma) in the microstructure of the Ni-La catalyst. Similarly, catalytic dry reforming of CH_4 was experimentally tested in a plasma micro-reactor using noble metals (Pt, Ag) or Ni [232]. Hot plasma was generated by an AC power source at 10 kHz and tunable voltage of 0–30 kV. The highest conversion of reactants (CO_2 and CH_4), up to 27.6%, was obtained for the Ag catalyst. The authors reported the need to achieve a good understanding of the mechanism of plasma activation of the catalysts.

Microwave reforming was also tested for biogas, investigating the effect of the presence of nitrogen and oxygen in the reaction mixture, and it was found that their presence may improve methane conversion [233].

Gray et al. [234] applied a positive electric field on a pure metallic Ni-foam-catalyst bed and observed that the positive field promotes the oxidation of the Ni catalyst and increases methane activation and conversion while preventing coking. They attributed the improved performance to the water adhesion to the catalyst surface and water activation in the bulk catalyst, both promoted in the presence of an electric field. Oxide formation, as well as the presence of the electric field itself, also inhibits carbon polymerization.

Electrically assisted processes represent a very interesting challenge for exploiting electricity produced in excess during peak periods, especially of solar origin, and thermochemically converting methane or biomethane into hydrogen with high-scale flexibility.

8.3. Multistage Processes

The implementation of complex process schemes may override limited performances in heat/mass transfer or catalysts, according to the more general principles of process

intensification. For instance, a multistage FB plant can largely reduce the typical back-mixing behavior of such technology [235], leading to well-controlled residence times and product yields. A multistage strategy can also contribute to complex reaction decoupling, when different reaction paths are possible, by selecting at each stage optimal operating conditions and a suitable catalyst [236].

Hydrogen production via steam reforming in an interconnected fluidized bed has been modelled [237]. Although the authors were mainly focused on a good estimation of fluid-dynamic behavior and drag mode, the investigation lays the basis for a possible application of a multistage plant on an industrial scale.

A two-zone fluidized-bed-reactor coupling permselective Pd/Ag membranes was experimentally investigated at lab-scale [238] to intensify the process for producing pure hydrogen by biogas DR. Compared to a single-stage process, the 2-zone FB reactor is more stable, thanks to the regeneration of the catalyst in the lower section of the system. Coupling a membrane leads to improvements in H_2 yield and purity. Along these lines, a 2-zone FB reactor and 2-zone FB reactor with membranes were mathematically modelled [239] and the model predicted well the in situ regeneration of the catalyst in the lower zone of the fluidized bed.

For gas mixture purification, a multistage FB can effectively perform as an absorber by strongly limiting bypass phenomena and easily tackling issues connected to temperature control. This option was successfully investigated for sour gas purification by chemisorption [240] and would be applied to syngas treatment by tuning the adsorbent characteristics, e.g., for CO removal [241].

In conclusion, the multistage reactor configurations allow for the intensification of the plant productivity and for overcoming the fluid dynamic limits due to the back-mixing of the reactants and products, for example, in multiphase systems.

8.4. Hydrogen Purification by Membranes

Membrane-based processes for gas separation or purification are attractive for their low environmental footprint, intrinsic safety, and modular nature with respect to traditional technologies, essentially based on chemical absorption [242]. Hydrogen separation can be accomplished at low temperatures by polymeric membranes [243,244], whose performance, limits, and perspectives were recently reviewed [245]. In glassy polymeric membranes (e.g., cellulose acetate and polysulfone), the selectivity towards N_2 and CH_4 is high enough (50–100), but it drastically decays towards CO_2. Furthermore, the use at high temperatures is prevented by the decomposition of the polymers at medium-high temperatures.

One of the major concerns about the use of membrane technology for hydrogen separation is mainly related to the intrinsic limitation in meeting the requested purity of the hydrogen (well above 99%) and recovery (around 60%). Gas separation by membrane, indeed, can hardly reach those purity thresholds with an economically sustainable process (i.e., a limited number of membrane stages).

For this reason, the coupled membrane and PSA process was experimentally investigated [246] for recovery of H_2 from industrial streams (syngas, coke gas, petrochemical, etc.). A major part of the impurities (CO, N_2, etc.) was removed at the membrane stage, whilst CO_2 and H_2 were separated by PSA, and the hydrogen purity could thus be enhanced as high as 99.9 or 99.99%, as requested. The proposed process exhibited enhanced performance in comparison to the purely membrane step.

Membranes for high-temperature (higher than 600 °C) separation of H_2 via protonic exchange are based on a thin Pd film deposited over microporous ceramic or metallic support, achieving H_2/N_2 selectivity up to 10^4 [247]. Unfortunately, the presence of CO in the gas mixture gives rise to poisoning and the lowering of hydrogen permeability [248]. Catalano et al. [249] theoretically investigated such a phenomenon, assuming a CO competition with H_2 in the covering of the active sites by adsorption, which is a preliminary stage for permeation through the metal film. Their model can estimate the effect of temperature, thickness and CO molar fraction on permeation rate in Pd membranes.

Ceramic membranes can represent a valid alternative compared to the use of precious metals for the separation of hydrogen at high temperatures, allowing for the configuring of a reforming reactor that is improved by the separation of the product. Microporous membranes are already commercially available, though with limited selectivity. Hybrid silica membranes were modified by chemical vapor infiltration [250] to increase the hydrogen selectivity towards CO_2 and CH_4, achieving values of 61.3 and 460.5 at 250 °C, respectively.

A novel proton–ceramic membrane (MPEC) has been developed and tested at 750 °C [251] for hydrogen separation from syngas. Stable permeation was measured in an asymmetric configuration for 100 h, using a sweep gas downstream. Despite the rather complex protocol of synthesis, the membrane cost could result in being largely lower than that of the Pd-based membranes, with respect to which they have similar high selectivity.

Residual CO_2 in syngas can be separated at low temperatures by well-established methods based on adsorption [252] or membranes [253]. In this respect, an innovative membrane-based module for the gas separation has been developed and tested at lab-scale by Minelli et al. [254]. The process was based on alternating steps of permeation and adsorption, resulting in an improvement in the effective separation factor. The characteristic times represent a further operation variable of the process that can purposely change the average purity or flow rate of the permeates, without modifying the membrane configuration. This device could find application in the separation of CO_2 from syngas, if applied downstream of a reformer.

In summary, the syngas purification can be carried out either by removing the non-hydrogen species or by separating H_2 through proton-transport membranes. The latter represent an expensive alternative because they are based on noble metals, but the recent development of ceramic membranes may represent a promising alternative for the in-line H_2 separation during the methane and bio-methane reforming.

8.5. Catalyst Patterning

In conventional tubular autothermal reformers, a partial oxidation reaction is carried out first at the inlet of the reactor and is then followed by the steam-reforming or dry-reforming reaction [136]. As mentioned previously in Section 5, the highly exothermic and fast oxidation reaction at the inlet of the reactor can cause the temperature of this zone to rapidly increase and creates a non-homogeneous temperature profile which hinders reactant conversion and catalyst stability by forming hot spots and cold zones [139,255]. Non-isothermicity is also a problem for conventional packed-bed steam-reforming reactors, due to heat-exchange limitations [256,257], and PO, DR and the dual-reforming process can be expected to suffer from similar problems. While fluidized beds can offer a solution in terms of heat- and mass-transfer optimization [258], they also add complexity to reaction operation and catalyst selection compared to fixed-bed reactors, as factors such as the control of a correct fluidization regime and attrition resistance of catalyst and reactor components have to be considered [259,260]. Therefore, improvement in the performance of fixed-bed reactors is particularly interesting for future developments. Patterned fixed beds [261,262], which is to say beds where layers of different catalytic activity are regularly distributed inside the reactor, may offer a simple solution to improving the performance of reforming reactors, with different possible configurations that have recently been evaluated. For steam reformers, axially alternating layers of catalyst material with metallic foam layers [263] can potentially greatly decreases the temperature gradient inside the reformer reactor. Even though a patterned-bed reactor intuitively contains less catalyst compared to a conventional packed bed of the same size, simulation results suggest that even halving the mass of catalyst reduced the methane conversion rate by only 15%, suggesting the possibility of obtaining high conversion even with a lower catalyst load. Radial patterning of the catalyst, as opposed to axial layering, appears to be a more promising solution, as numerical investigation indicates a capability of achieving an increase in methane conversion while lowering the required catalyst mass (10.6% increase in conversion with a 26.16% decrease in catalyst load) [264]. Crucial aspects of optimization of the process

consist in determining the number of layers, their size and the catalyst-to-gap ratio [265]. For an optimized radially patterned biogas dual reformer, a reduction in catalyst load of 41% with no adverse effect on reactant conversion was predicted, displaying great benefits of this configuration also in reducing cost, compared to conventional reformers [266]. Lee et al. [267] observed that optimized axial alternation of layers of a steam-reforming and dry-reforming catalyst can greatly help to reduce the carbon deposition problem associated with the dry- or dual-reforming process for biogas, while at the same time displaying great potential for reduction in capital and energy costs of the reformer.

An interesting alternative to removing temperature and mass-transfer gradients is to pattern the distribution of the catalyst particle diameter in multichannel reactors [268]. Patterning alternating preheated catalyst sections has also been evaluated [269].

The patterning of catalysts also proved beneficial in simulation work on ATSR process, with radially patterned reactors offering best performance enhancement with reduced catalyst load and oxygen demand [270–272]. Interestingly, patterning of catalysts can also potentially be achieved in novel and compact plate reactors [273]. Finally, a patterned reactor could also be operated with the use of membranes, either for separation of reaction zones in dual reforming [274] or to improve hydrogen yield and separation in steam reforming [275].

In conclusion, the patterning of catalysts makes it possible to considerably reduce the non-isothermal effects due to the succession of different reactions during the CH_4 reforming. The development of such catalysts represents a very interesting challenge for improving the performance and efficiency of fixed-bed catalytic reactors.

9. Conclusions

Steam reforming is currently the most diffused process for H_2 production on an industrial scale and has the lowest price (between 1.0 and 2.0 USD/kg), making use of catalysts essentially based on nickel. The current research is principally oriented towards the development of new catalysts, with the aim of reducing the negative impact of Ni compounds with respect to the environment and health. Iron, in combination with Ni, appears to be an effective element for improving catalyst performance and safety.

Due to the increased relevancy of carbon capture and decarbonization, dry reforming of hydrocarbons is a suitable option for conversion of CO_2 in syngas. The process is highly allothermal, and needs an energy supply of heat or electricity. In this respect, microwave- or plasma-assisted reactors deserve a large amount of interest for future development. While substantial work has been carried out on catalysts, the process is yet to achieve sufficient maturity for industrial application.

Partial oxidation of methane is an exothermic reaction, where the use of a catalyst allows for a lower reaction temperature and increased selectivity. On an industrial scale, the process requires pure oxygen and may experience problems related to temperature run-off. Very interestingly, the application of chemical looping schemes with the use of an oxygen carrier can avoid the use of an air-separation unit, moving this process to a lower and more-distributed industrial scale for hydrogen generation, with high-scale flexibility.

Thermo-catalytic decomposition of methane is a further process for producing H_2 and carbon, with a slightly endothermic reaction. The technology is easy to implement, also at small scale, using catalysts based on Ni or Cu, the latter being non- toxic. The main issue is catalyst regeneration because of deactivation by carbon deposition, an aspect that poses challenges in process optimization and intensification.

For all the above reported processes, the implementation of more complex reactor schemes (multistage, membrane/adsorption coupling, chemical looping, etc.) could improve the process efficiency, scalability, and flexibility. The utilization of fluidized-bed technology would be helpful for some related catalyst/carrier issues, such as regeneration, circulation, and discharging, as well as for largely improving the heat-transfer rate, and also for the utilization of an external energy source (e.g., solar). In such a context, the

application of catalyst patterning is another effective way to tackle problems of temperature distribution and instabilities along the reformer.

Funding: The research has been funded by the Italian National Programme "Ricerca e Sviluppo di Tecnologie per la Filiera dell'Idrogeno—AdP Italian Ministery MiTE—ENEA, Mission 2, Comp. 2.3.5, PNRR, 2022–2025, L.A. 1.1.25".

Conflicts of Interest: The authors declare no conflict of interest.

Abbreviations

CL	chemical looping
CL-DRM	Chemical-cooping dry reforming of methane
CRM	critical raw material
DR	dry reforming
ATSR	autothermal steam reforming
ATDR	autothermal dry reforming
2-R	dual reforming
TR	tri-reforming
CCS	carbon capture and storage
DFT	density functional theory
FB	fluidized bed
MPEC	mixed-conducting ceramic–ceramic composite
MW	microwave
NG	natural gas
OC	oxygen carrier
PO	partial oxidation
PSA	pressure swing adsorption
SR	steam reforming
TCD	thermo-catalytic decomposition
TGA	thermo-gravimetric analysis
TPR	temperature-programmed reduction
WGS	water gas shift

References

1. Abdin, Z.; Zafaranloo, A.; Rafiee, A.; Mérida, W.; Lipiński, W.; Khalilpour, K.R. Hydrogen as an Energy Vector. *Renew. Sustain. Energy Rev.* **2020**, *120*, 109620. [CrossRef]
2. International Energy Agency (IEA). *The Future of Hydrogen*; IEA: Paris, France, 2019.
3. Riera, J.A.; Lima, R.M.; Knio, O.M. A Review of Hydrogen Production and Supply Chain Modeling and Optimization. *Int. J. Hydrogen Energy* **2023**, *48*, 13731–13755. [CrossRef]
4. Rasul, M.G.; Hazrat, M.A.; Sattar, M.A.; Jahirul, M.I.; Shearer, M.J. The Future of Hydrogen: Challenges on Production, Storage and Applications. *Energy Convers. Manag.* **2022**, *272*, 116326. [CrossRef]
5. Ishaq, H.; Dincer, I.; Crawford, C. A Review on Hydrogen Production and Utilization: Challenges and Opportunities. *Int. J. Hydrogen Energy* **2022**, *47*, 26238–26264. [CrossRef]
6. Okolie, J.A.; Patra, B.R.; Mukherjee, A.; Nanda, S.; Dalai, A.K.; Kozinski, J.A. Futuristic Applications of Hydrogen in Energy, Biorefining, Aerospace, Pharmaceuticals and Metallurgy. *Int. J. Hydrogen Energy* **2021**, *46*, 8885–8905. [CrossRef]
7. Capurso, T.; Stefanizzi, M.; Torresi, M.; Camporeale, S.M. Perspective of the Role of Hydrogen in the 21st Century Energy Transition. *Energy Convers. Manag.* **2022**, *251*, 114898. [CrossRef]
8. Arcos, J.M.M.; Santos, D.M.F. The Hydrogen Color Spectrum: Techno-Economic Analysis of the Available Technologies for Hydrogen Production. *Gases* **2023**, *3*, 25–46. [CrossRef]
9. Monteiro, E.; Brito, P.S.D. Hydrogen Supply Chain: Current Status and Prospects. *Energy Storage* **2023**, e466. [CrossRef]
10. Bridgwater, A. V Renewable Fuels and Chemicals by Thermal Processing of Biomass. *Chem. Eng. J.* **2003**, *91*, 87–102. [CrossRef]
11. Incer-Valverde, J.; Korayem, A.; Tsatsaronis, G.; Morosuk, T. "Colors" of Hydrogen: Definitions and Carbon Intensity. *Energy Convers. Manag.* **2023**, *291*, 117294. [CrossRef]
12. Qureshi, F.; Yusuf, M.; Kamyab, H.; Vo, D.V.N.; Chelliapan, S.; Joo, S.W.; Vasseghian, Y. Latest Eco-Friendly Avenues on Hydrogen Production towards a Circular Bioeconomy: Currents Challenges, Innovative Insights, and Future Perspectives. *Renew. Sustain. Energy Rev.* **2022**, *168*, 112916. [CrossRef]
13. Borowski, P.F.; Karlikowska, B. Clean Hydrogen Is a Challenge for Enterprises in the Era of Low-Emission and Zero-Emission Economy. *Energies* **2023**, *16*, 1171. [CrossRef]

14. AlHumaidan, F.S.; Absi Halabi, M.; Rana, M.S.; Vinoba, M. Blue Hydrogen: Current Status and Future Technologies. *Energy Convers. Manag.* **2023**, *283*, 116840. [CrossRef]
15. Angeli, S.D.; Monteleone, G.; Giaconia, A.; Lemonidou, A.A. State-of-the-Art Catalysts for CH_4 Steam Reforming at Low Temperature. *Int. J. Hydrogen Energy* **2014**, *39*, 1979–1997. [CrossRef]
16. Summa, P.; Samojeden, B.; Motak, M. Dry and Steam Reforming of Methane. Comparison and Analysis of Recently Investigated Catalytic Materials. A Short Review. *Pol. J. Chem. Technol.* **2019**, *21*, 31–37. [CrossRef]
17. Fan, Z.; Weng, W.; Zhou, J.; Gu, D.; Xiao, W. Catalytic Decomposition of Methane to Produce Hydrogen: A Review. *J. Energy Chem.* **2021**, *58*, 415–430. [CrossRef]
18. Chung, W.T.; Mekhemer, I.M.A.; Mohamed, M.G.; Elewa, A.M.; EL-Mahdy, A.F.M.; Chou, H.H.; Kuo, S.W.; Wu, K.C.W. Recent Advances in Metal/Covalent Organic Frameworks Based Materials: Their Synthesis, Structure Design and Potential Applications for Hydrogen Production. *Coord. Chem. Rev.* **2023**, *483*, 215066. [CrossRef]
19. Saeidi, S.; Sápi, A.; Khoja, A.H.; Najari, S.; Ayesha, M.; Kónya, Z.; Asare-Bediako, B.B.; Tatarczuk, A.; Hessel, V.; Keil, F.J.; et al. Evolution Paths from Gray to Turquoise Hydrogen via Catalytic Steam Methane Reforming: Current Challenges and Future Developments. *Renew. Sustain. Energy Rev.* **2023**, *183*, 113392. [CrossRef]
20. Ganguli, A.; Bhatt, V. Hydrogen Production Using Advanced Reactors by Steam Methane Reforming: A Review. *Front. Therm. Eng.* **2023**, *3*, 1143987. [CrossRef]
21. Yang, W.W.; Ma, X.; Tang, X.Y.; Dou, P.Y.; Yang, Y.J.; He, Y.L. Review on Developments of Catalytic System for Methanol Steam Reforming from the Perspective of Energy-Mass Conversion. *Fuel* **2023**, *345*, 128234. [CrossRef]
22. Qin, T.; Yuan, S. Research Progress of Catalysts for Catalytic Steam Reforming of High Temperature Tar: A Review. *Fuel* **2023**, *331*, 125790. [CrossRef]
23. Deng, Y.; Li, S.; Appels, L.; Zhang, H.; Sweygers, N.; Baeyens, J.; Dewil, R. Steam Reforming of Ethanol by Non-Noble Metal Catalysts. *Renew. Sustain. Energy Rev.* **2023**, *175*, 113184. [CrossRef]
24. Yadav, A.K.; Vaidya, P.D. A Review on Butanol Steam Reforming for Renewable Hydrogen Production. *J. Indian Chem. Soc.* **2023**, *100*, 101050. [CrossRef]
25. Amjad, U.E.S.; Quintero, C.W.M.; Ercolino, G.; Italiano, C.; Vita, A.; Specchia, S. Methane Steam Reforming on the Pt/CeO_2 Catalyst: Effect of Daily Start-Up and Shut-Down on Long-Term Stability of the Catalyst. *Ind. Eng. Chem. Res.* **2019**, *58*, 16395–16406. [CrossRef]
26. Androulakis, A.; Yentekakis, I.V.; Panagiotopoulou, P. Dry Reforming of Methane over Supported Rh and Ru Catalysts: Effect of the Support (Al_2O_3, TiO_2, ZrO_2, YSZ) on the Activity and Reaction Pathway. *Int. J. Hydrogen Energy* 2023, *in press*. [CrossRef]
27. Geng, H.; Zhao, H.; Yu, S.; Li, D.; Lei, H.; Zhang, Y. High Performance of Conversion and Selectivity of Methane to CO via Pt-Pd Core-Shell Structural Catalyst. *Appl. Catal. B* **2023**, *324*, 122189. [CrossRef]
28. Singh, A.K.; Pal, P.; Rathore, S.S.; Sahoo, U.K.; Sarangi, P.K.; Prus, P.; Dziekański, P. Sustainable Utilization of Biowaste Resources for Biogas Production to Meet Rural Bioenergy Requirements. *Energies* **2023**, *16*, 5409. [CrossRef]
29. Yin, W.; Guilhaume, N.; Schuurman, Y. Model Biogas Reforming over $Ni\text{-}Rh/MgAl_2O_4$ Catalyst. Effect of Gas Impurities. *Chem. Eng. J.* **2020**, *398*, 125534. [CrossRef]
30. Chaghouri, M.; Hany, S.; Cazier, F.; Tidahy, H.L.; Gennequin, C.; Abi-Aad, E. Impact of Impurities on Biogas Valorization through Dry Reforming of Methane Reaction. *Int. J. Hydrogen Energy* **2022**, *47*, 40415–40429. [CrossRef]
31. Postels, S.; Abánades, A.; von der Assen, N.; Rathnam, R.K.; Stückrad, S.; Bardow, A. Life Cycle Assessment of Hydrogen Production by Thermal Cracking of Methane Based on Liquid-Metal Technology. *Int. J. Hydrogen Energy* **2016**, *41*, 23204–23212. [CrossRef]
32. Osman, A.I.; Mehta, N.; Elgarahy, A.M.; Hefny, M.; Al-Hinai, A.; Al-Muhtaseb, A.H.; Rooney, D.W. Hydrogen Production, Storage, Utilisation and Environmental Impacts: A Review. *Environ. Chem. Lett.* **2022**, *20*, 153–188. [CrossRef]
33. Gholkar, P.; Shastri, Y.; Tanksale, A. Renewable Hydrogen and Methane Production from Microalgae: A Techno-Economic and Life Cycle Assessment Study. *J. Clean. Prod.* **2021**, *279*, 123726. [CrossRef]
34. Ji, M.; Wang, J. Review and Comparison of Various Hydrogen Production Methods Based on Costs and Life Cycle Impact Assessment Indicators. *Int. J. Hydrogen Energy* **2021**, *46*, 38612–38635. [CrossRef]
35. Megia, P.J.; Vizcaino, A.J.; Calles, J.A.; Carrero, A. Hydrogen Production Technologies: From Fossil Fuels toward Renewable Sources. A Mini Review. *Energy Fuels* **2021**, *35*, 16403–16415. [CrossRef]
36. Faye, O.; Szpunar, J.; Eduok, U. A Critical Review on the Current Technologies for the Generation, Storage, and Transportation of Hydrogen. *Int. J. Hydrogen Energy* **2022**, *47*, 13771–13802. [CrossRef]
37. Chen, L.; Qi, Z.; Zhang, S.; Su, J.; Somorjai, G.A. Catalytic Hydrogen Production from Methane: A Review on Recent Progress and Prospect. *Catalysts* **2020**, *10*, 858. [CrossRef]
38. Boretti, A.; Banik, B.K. Advances in Hydrogen Production from Natural Gas Reforming. *Adv. Energy Sustain. Res.* **2021**, *2*, 2100097. [CrossRef]
39. Suleman, F.; Dincer, I.; Agelin-Chaab, M. Environmental Impact Assessment and Comparison of Some Hydrogen Production Options. *Int. J. Hydrogen Energy* **2015**, *40*, 6976–6987. [CrossRef]
40. IRENA. Hydrogen (IRENA). Available online: https://www.irena.org/Energy-Transition/Technology/Hydrogen#:~:text=As%20at%20the%20end%20of,around%204%25%20comes%20from%20electrolysis (accessed on 24 August 2023).

41. Wang, J.; Liu, Z.; Ji, C.; Liu, L. Heat Transfer and Reaction Characteristics of Steam Methane Reforming in a Novel Composite Packed Bed Microreactor for Distributed Hydrogen Production. *Energies* **2023**, *16*, 4347. [CrossRef]
42. Levalley, T.L.; Richard, A.R.; Fan, M. The Progress in Water Gas Shift and Steam Reforming Hydrogen Production Technologies—A Review. *Int. J. Hydrogen Energy* **2014**, *39*, 16983–17000. [CrossRef]
43. Kaiwen, L.; Bin, Y.; Tao, Z. Economic Analysis of Hydrogen Production from Steam Reforming Process: A Literature Review. *Energy Sources Part B Econ. Plan. Policy* **2018**, *13*, 109–115. [CrossRef]
44. Ozbilen, A.; Dincer, I.; Rosen, M.A. Comparative Environmental Impact and Efficiency Assessment of Selected Hydrogen Production Methods. *Environ. Impact Assess. Rev.* **2013**, *42*, 1–9. [CrossRef]
45. Argyris, P.A.; Wright, A.; Taheri Qazvini, O.; Spallina, V. Dynamic Behaviour of Integrated Chemical Looping Process with Pressure Swing Adsorption in Small Scale On-Site H_2 and Pure CO_2 Production. *Chem. Eng. J.* **2022**, *428*, 132606. [CrossRef]
46. Ochoa Bique, A.; Maia, L.K.K.; La Mantia, F.; Manca, D.; Zondervan, E. Balancing Costs, Safety and CO_2 Emissions in the Design of Hydrogen Supply Chains. *Comput. Chem. Eng.* **2019**, *129*, 106493. [CrossRef]
47. Sehested, J. Sintering of Nickel Steam-Reforming Catalysts. *J. Catal.* **2003**, *217*, 417–426. [CrossRef]
48. Sengodan, S.; Lan, R.; Humphreys, J.; Du, D.; Xu, W.; Wang, H.; Tao, S. Advances in Reforming and Partial Oxidation of Hydrocarbons for Hydrogen Production and Fuel Cell Applications. *Renew. Sustain. Energy Rev.* **2018**, *82*, 761–780. [CrossRef]
49. Meloni, E.; Martino, M.; Palma, V. A Short Review on Ni Based Catalysts and Related Engineering Issues for Methane Steam Reforming. *Catalysts* **2020**, *10*, 352. [CrossRef]
50. Salcedo, A.; Lustemberg, P.G.; Rui, N.; Palomino, R.M.; Liu, Z.; Nemsak, S.; Senanayake, S.D.; Rodriguez, J.A.; Ganduglia-Pirovano, M.V.; Irigoyen, B. Reaction Pathway for Coke-Free Methane Steam Reforming on a Ni/CeO_2 Catalyst: Active Sites and the Role of Metal-Support Interactions. *ACS Catal.* **2021**, *11*, 8327–8337. [CrossRef] [PubMed]
51. Han, B.; Wang, F.; Zhang, L.; Wang, Y.; Fan, W.; Xu, L.; Yu, H.; Li, Z. Syngas Production from Methane Steam Reforming and Dry Reforming Reactions over Sintering-Resistant Ni@SiO_2 Catalyst. *Res. Chem. Intermed.* **2020**, *46*, 1735–1748. [CrossRef]
52. Jeon, K.W.; Kim, J.K.; Kim, B.J.; Jang, W.J.; Kang, Y.C.; Roh, H.S. Ultra-Stable Porous Yolk-Shell Ni Catalysts for the Steam Reforming of Methane with Alkali Poisoning. *Chem. Eng. J.* **2023**, *454*, 140060. [CrossRef]
53. Wang, S.; Nabavi, S.A.; Clough, P.T. A Review on Bi/Polymetallic Catalysts for Steam Methane Reforming. *Int. J. Hydrogen Energy* **2023**, *48*, 15879–15893. [CrossRef]
54. Djaidja, A.; Messaoudi, H.; Kaddeche, D.; Barama, A. Study of Ni-M/MgO and Ni-M-Mg/Al (M=Fe or Cu) Catalysts in The CH_4-CO_2 and CH_4-H_2O Reforming. *Int. J. Hydrogen Energy* **2015**, *40*, 4989–4995. [CrossRef]
55. Lu, H.; Shi, X.; Costa, M.; Huang, C. Carcinogenic Effect of Nickel Compounds. *Mol. Cell Biochem.* **2005**, *279*, 45–67. [CrossRef]
56. Al-Mamoori, A.; Krishnamurthy, A.; Rownaghi, A.A.; Rezaei, F. Carbon Capture and Utilization Update. *Energy Technol.* **2017**, *5*, 834–849. [CrossRef]
57. Joos, L.; Huck, J.M.; Van Speybroeck, V.; Smit, B. Cutting the Cost of Carbon Capture: A Case for Carbon Capture and Utilization. *Faraday Discuss.* **2016**, *192*, 391–414. [CrossRef] [PubMed]
58. Rackley, S.A. Overview of Carbon Capture and Storage. In *Carbon Capture and Storage*; Butterworth-Heinemann: Oxford, UK, 2017; pp. 23–36, ISBN 9780128120415.
59. Alvarado, V.; Manrique, E. Enhanced Oil Recovery: An Update Review. *Energies* **2010**, *3*, 1529–1575. [CrossRef]
60. Gao, Y.; Jiang, J.; Meng, Y.; Yan, F.; Aihemaiti, A. A Review of Recent Developments in Hydrogen Production via Biogas Dry Reforming. *Energy Convers. Manag.* **2018**, *171*, 133–155. [CrossRef]
61. Jung, S.; Lee, J.; Moon, D.H.; Kim, K.H.; Kwon, E.E. Upgrading Biogas into Syngas through Dry Reforming. *Renew. Sustain. Energy Rev.* **2021**, *143*, 110949. [CrossRef]
62. Minh, D.P.; Siang, T.J.; Vo, D.V.N.; Phan, T.S.; Ridart, C.; Nzihou, A.; Grouset, D. Hydrogen Production from Biogas Reforming: An Overview of Steam Reforming, Dry Reforming, Dual Reforming, and Tri-Reforming of Methane. In *Hydrogen Supply Chain: Design, Deployment and Operation*; Elsevier: Amsterdam, The Netherlands, 2018; pp. 111–166, ISBN 9780128111970.
63. Aramouni, N.A.K.; Touma, J.G.; Tarboush, B.A.; Zeaiter, J.; Ahmad, M.N. Catalyst Design for Dry Reforming of Methane: Analysis Review. *Renew. Sustain. Energy Rev.* **2018**, *82*, 2570–2585. [CrossRef]
64. Yan, W.; Chuan, T.; Ching, J.; Lee, D.; Chang, J. Bioresource Technology Biorefineries of Carbon Dioxide: From Carbon Capture and Storage (CCS) to Bioenergies Production. *Bioresour. Technol.* **2016**, *215*, 346–356. [CrossRef]
65. Aramouni, N.A.K. Carbon Mitigation in the Dry Reforming of Methane. Ph.D. Thesis, University of Limerick, Limerick, Ireland, 2020.
66. González-Castaño, M.; Dorneanu, B.; Arellano-García, H. The Reverse Water Gas Shift Reaction: A Process Systems Engineering Perspective. *React. Chem. Eng.* **2021**, *6*, 954–976. [CrossRef]
67. Abdulrasheed, A.; Jalil, A.A.; Gambo, Y.; Ibrahim, M.; Hambali, H.U.; Shahul Hamid, M.Y. A Review on Catalyst Development for Dry Reforming of Methane to Syngas: Recent Advances. *Renew. Sustain. Energy Rev.* **2019**, *108*, 175–193. [CrossRef]
68. Phan, T.S.; Pham Minh, D. New Performing Hydroxyapatite-Based Catalysts in Dry-Reforming of Methane. *Int. J. Hydrogen Energy* **2023**, *48*, 30770–30790. [CrossRef]
69. Nakajima, E.A.; Oliveira, L.G.; Gasparrini, L.J.; de Queiros Souza, G.E.; Ignacio, A.A.; Alves, H.J.; Borba, C.E. Kinetics of Dry Reforming of Methane Catalyzed by Ni/Si-MCM-41. *Int. J. Hydrogen Energy* 2023, *in press*. [CrossRef]
70. Zhang, Y.; Zhang, G.; Liu, J.; Li, T.; Wang, Y.; Zhao, Y.; Li, G.; Zhang, Y. Dry Reforming of Methane over Ni/SiO_2 Catalysts: Role of Support Structure Properties. *Fuel* **2023**, *340*, 127490. [CrossRef]

71. Song, Q.; Ran, R.; Wu, X.; Si, Z.; Weng, D. Dry Reforming of Methane over Ni Catalysts Supported on Micro- and Mesoporous Silica. *J. CO2 Util.* **2023**, *68*, 102387. [CrossRef]
72. Li, S.; Fu, Y.; Kong, W.; Wang, J.; Yuan, C.; Pan, B.; Zhu, H.; Chen, X.; Zhang, Y.; Zhang, J.; et al. Tuning Strong Metal-Support Interactions to Boost Activity and Stability of Aluminium Nitride Supported Nickel Catalysts for Dry Reforming of Methane. *Fuel* **2023**, *343*, 127918. [CrossRef]
73. Haug, L.; Thurner, C.; Bekheet, M.F.; Ploner, K.; Bischoff, B.; Gurlo, A.; Kunz, M.; Sartory, B.; Penner, S.; Klötzer, B. Pivotal Role of Ni/ZrO_2 Phase Boundaries for Coke-Resistant Methane Dry Reforming Catalysts. *Catalysts* **2023**, *13*, 804. [CrossRef]
74. Zhang, X.; Shen, Y.; Liu, Y.; Zheng, J.; Deng, J.; Yan, T.; Cheng, D.; Zhang, D. Unraveling the Unique Promotion Effects of a Triple Interface in Ni Catalysts for Methane Dry Reforming. *Ind. Eng. Chem. Res.* **2023**, *62*, 4965–4975. [CrossRef]
75. Georgiadis, A.G.; Siakavelas, G.I.; Tsiotsias, A.I.; Charisiou, N.D.; Ehrhardt, B.; Wang, W.; Sebastian, V.; Hinder, S.J.; Baker, M.A.; Mascotto, S.; et al. Biogas Dry Reforming over Ni/LnOx-Type Catalysts (Ln = La, Ce, Sm or Pr). *Int. J. Hydrogen Energy* **2023**, *48*, 19953–19971. [CrossRef]
76. Li, T.; Wang, J.; Zhang, G.; Liu, J.; Wang, Y.; Zhao, Y.; Li, G.; Lv, Y. Effects of Promoter and Calcination Temperatures on the Catalytic Performance of Y Promoted Co/WC-AC for Dry Reforming of Methane. *Chem. Asian J.* **2023**, *18*, e202300319. [CrossRef] [PubMed]
77. Ewbank, J.L.; Kovarik, L.; Kenvin, C.C.; Sievers, C. Effect of Preparation Methods on the Performance of Co/Al_2O_3 Catalysts for Dry Reforming of Methane. *Green Chem.* **2014**, *16*, 885–896. [CrossRef]
78. Mohd Jailani, M.S.A.; Miskan, S.N.; Bahari, M.B.; Setiabudi, H.D. Optimization of Dry Reforming of Methane over Yttrium Oxide-Cobalt/Mesoporous Alumina Using Response Surface Methodology. *Mater. Today Proc.* 2023, *in press*. [CrossRef]
79. Owgi, A.H.K.; Jalil, A.A.; Aziz, M.A.A.; Nabgan, W.; Alhassan, M.; Sofi, M.H.M.; Hassan, N.S.; Saravanan, R.; Bahari, M.B. Methane Dry Reforming on Fibrous Silica-Alumina Employing Nanocrystals of Nickel and Cobalt to Recognize the Most Efficient Metal. *Int. J. Hydrogen Energy* 2023, *in press*. [CrossRef]
80. Zafarnak, S.; Rahimpour, M.R. Co-Ni Bimetallic Supported on Mullite as a Promising Catalyst for Biogas Dry Reforming toward Hydrogen Production. *Mol. Catal.* **2023**, *534*, 112803. [CrossRef]
81. Liang, D.; Wang, Y.; Chen, M.; Xie, X.; Li, C.; Wang, J.; Yuan, L. Dry Reforming of Methane for Syngas Production over Attapulgite-Derived MFI Zeolite Encapsulated Bimetallic Ni-Co Catalysts. *Appl. Catal. B* **2023**, *322*, 122088. [CrossRef]
82. Theofanidis, S.A.; Galvita, V.V.; Poelman, H.; Marin, G.B. Enhanced Carbon-Resistant Dry Reforming Fe-Ni Catalyst: Role of Fe. *ACS Catal.* **2015**, *5*, 3028–3039. [CrossRef]
83. Li, Y.; Wang, Q.; Cao, M.; Li, S.; Song, Z.; Qiu, L.; Yu, F.; Li, R.; Yan, X. Structural Evolution of Robust Ni_3Fe_1 Alloy on Al_2O_3 in Dry Reforming of Methane: Effect of Iron-Surplus Strategy from Ni_1Fe_1 to Ni_3Fe_1. *Appl. Catal. B* **2023**, *331*, 122669. [CrossRef]
84. Chatla, A.; Ghouri, M.M.; El Hassan, O.W.; Mohamed, N.; Prakash, A.V.; Elbashir, N.O. An Experimental and First Principles DFT Investigation on the Effect of Cu Addition to Ni/Al_2O_3 Catalyst for the Dry Reforming of Methane. *Appl. Catal. A Gen.* **2020**, *602*, 117699. [CrossRef]
85. Han, K.; Wang, S.; Liu, Q.; Wang, F. Optimizing the Ni/Cu Ratio in Ni-Cu Nanoparticle Catalysts for Methane Dry Reforming. *ACS Appl. Nano Mater.* **2021**, *4*, 5340–5348. [CrossRef]
86. Khan, M.A.; Challiwala, M.S.; Prakash, A.V.; Elbashir, N.O. Conceptual Modeling of a Reactor Bed of a Nickel-Copper Bi-Metallic Catalyst for Dry Reforming of Methane. *Chem. Eng. Sci.* **2023**, *267*, 118315. [CrossRef]
87. Gokhale, A.A.; Kandoi, S.; Greeley, J.P.; Mavrikakis, M.; Dumesic, J.A. Molecular-Level Descriptions of Surface Chemistry in Kinetic Models Using Density Functional Theory. *Chem. Eng. Sci.* **2004**, *59*, 4679–4691. [CrossRef]
88. Zhang, D.; Xie, H.; Chen, S.; Zeng, J.; Zhou, G. High-Performance CoCe Catalyst Constructed by the Glucose-Assisted In-Situ Reduction for CH_4/CO_2 Dry Reforming. *Fuel* **2023**, *344*, 128083. [CrossRef]
89. Loktev, A.S.; Arkhipova, V.A.; Bykov, M.A.; Sadovnikov, A.A.; Dedov, A.G. Novel Samarium Cobaltate/Silicon Carbide Composite Catalyst for Dry Reforming of Methane into Synthesis Gas. *Pet. Chem.* **2023**. [CrossRef]
90. Loktev, A.S.; Arkhipova, V.A.; Bykov, M.A.; Sadovnikov, A.A.; Dedov, A.G. Cobalt–Samarium Oxide Composite as a Novel High-Performance Catalyst for Partial Oxidation and Dry Reforming of Methane into Synthesis Gas. *Pet. Chem.* **2023**, *63*, 317–326. [CrossRef]
91. Song, Y.; Ozdemir, E.; Ramesh, S.; Adishev, A.; Subramanian, S.; Harale, A.; Albuali, M.; Fadhel, B.A.; Jamal, A.; Moon, D.; et al. Dry Reforming of Methane by Stable Ni-Mo Nanocatalysts on Single-Crystalline MgO. *Science* **2020**, *367*, 777–781. [CrossRef] [PubMed]
92. Zhao, B.; Yan, B.; Yao, S.; Xie, Z.; Wu, Q.; Ran, R.; Weng, D.; Zhang, C.; Chen, J.G. $LaFe_{0.9}Ni_{0.1}O_3$ Perovskite Catalyst with Enhanced Activity and Coke-Resistance for Dry Reforming of Ethane. *J. Catal.* **2018**, *358*, 168–178. [CrossRef]
93. Sutthiumporn, K.; Maneerung, T.; Kathiraser, Y.; Kawi, S. CO_2 Dry-Reforming of Methane over $La_{0.8}Sr_{0.2}Ni_{0.8}M_{0.2}O_3$ Perovskite (M = Bi, Co, Cr, Cu, Fe): Roles of Lattice Oxygen on C-H Activation and Carbon Suppression. *Int. J. Hydrogen Energy* **2012**, *37*, 11195–11207. [CrossRef]
94. Das, S.; Bhattar, S.; Liu, L.; Wang, Z.; Xi, S.; Spivey, J.J.; Kawi, S. Effect of Partial Fe Substitution in $La_{0.9}Sr_{0.1}NiO_3$ Perovskite-Derived Catalysts on the Reaction Mechanism of Methane Dry Reforming. *ACS Catal.* **2020**, *10*, 12466–12486. [CrossRef]
95. Wang, M.; Zhao, T.; Dong, X.; Li, M.; Wang, H. Effects of Ce Substitution at the A-Site of $LaNi_{0.5}Fe_{0.5}O_3$ Perovskite on the Enhanced Catalytic Activity for Dry Reforming of Methane. *Appl. Catal. B* **2018**, *224*, 214–221. [CrossRef]

96. Yao, X.; Cheng, Q.; Attada, Y.; Ould-Chikh, S.; Ramírez, A.; Bai, X.; Mohamed, H.O.; Li, G.; Shterk, G.; Zheng, L.; et al. Atypical Stability of Exsolved Ni-Fe Alloy Nanoparticles on Double Layered Perovskite for CO_2 Dry Reforming of Methane. *Appl. Catal. B* **2023**, *328*, 122479. [CrossRef]
97. York, A.P.E.; Xiao, T.; Green, M.L.H. Brief Overview of the Partial Oxidation of Methane to Synthesis Gas. *Top. Catal.* **2003**, *22*, 345–358. [CrossRef]
98. Makaryan, I.A.; Salgansky, E.A.; Arutyunov, V.S.; Sedov, I.V. Non-Catalytic Partial Oxidation of Hydrocarbon Gases to Syngas and Hydrogen: A Systematic Review. *Energies* **2023**, *16*, 2916. [CrossRef]
99. Kalamaras, C.M.; Efstathiou, A.M. Hydrogen Production Technologies: Current State and Future Developments. *Conf. Pap. Energy* **2013**, *2013*, 690627. [CrossRef]
100. Osman, A.I. Catalytic Hydrogen Production from Methane Partial Oxidation: Mechanism and Kinetic Study. *Chem. Eng. Technol.* **2020**, *43*, 641–648. [CrossRef]
101. Elbadawi, A.H.; Ge, L.; Li, Z.; Liu, S.; Wang, S.; Zhu, Z. Catalytic Partial Oxidation of Methane to Syngas: Review of Perovskite Catalysts and Membrane Reactors. *Catal. Rev. Sci. Eng.* **2021**, *63*, 1–67. [CrossRef]
102. Liu, H.; He, D. Recent Progress on Ni-Based Catalysts in Partial Oxidation of Methane to Syngas. *Catal. Surv. Asia* **2012**, *16*, 53–61. [CrossRef]
103. Barbero, J.; Penã, M.A.; Campos-Martin, J.M.; Fierro, J.L.G.; Arias, P.L. Support Effect in Supported Ni Catalysts on Their Performance for Methane Partial Oxidation. *Catal. Lett.* **2003**, *87*, 211–218. [CrossRef]
104. Asencios, Y.J.O.; Yigit, N.; Wicht, T.; Stöger-Pollach, M.; Lucrédio, A.F.; Marcos, F.C.F.; Assaf, E.M.; Rupprechter, G. Partial Oxidation of Bio-Methane over Nickel Supported on MgO–ZrO_2 Solid Solutions. *Top. Catal.* **2023**. [CrossRef]
105. Ma, Y.; Ma, Y.; Zhao, Z.; Hu, X.; Ye, Z.; Yao, J.; Buckley, C.E.; Dong, D. Comparison of Fibrous Catalysts and Monolithic Catalysts for Catalytic Methane Partial Oxidation. *Renew. Energy* **2019**, *138*, 1010–1017. [CrossRef]
106. Özdemir, H.; Faruk Öksüzömer, M.A. Synthesis of Al_2O_3, MgO and $MgAl_2O_4$ by Solution Combustion Method and Investigation of Performances in Partial Oxidation of Methane. *Powder Technol.* **2020**, *359*, 107–117. [CrossRef]
107. Khaleel, A.; Pillantakath, A.R.; Adamson, A. Significant Role of Well-Dispersed Fe^{2+} Ions in the Support of Ni Catalysts in Enhancing Coking Resistance during Partial Oxidation of Methane. *Int. J. Hydrogen Energy* 2023, *in press*. [CrossRef]
108. Moral, A.; Reyero, I.; Llorca, J.; Bimbela, F.; Gandía, L.M. Partial Oxidation of Methane to Syngas Using Co/Mg and Co/Mg-Al Oxide Supported Catalysts. *Catal. Today* **2019**, *33*, 259–267. [CrossRef]
109. Choya, A.; de Rivas, B.; González-Velasco, J.R.; Gutiérrez-Ortiz, J.I.; López-Fonseca, R. Oxidation of Lean Methane over Cobalt Catalysts Supported on Ceria/Alumina. *Appl. Catal. A Gen.* **2020**, *591*, 117381. [CrossRef]
110. Mosayebi, A.; Abedini, R. Effect of Synthesis Solution PH of Co/γ-Al_2O_3 Catalyst on Its Catalytic Properties for Methane Conversion to Syngas. *J. Fuel Chem. Technol.* **2018**, *46*, 311–318. [CrossRef]
111. Fakeeha, A.H.; Arafat, Y.; Ibrahim, A.A.; Shaikh, H.; Atia, H.; Abasaeed, A.E.; Armbruster, U.; Al-Fatesh, A.S. Highly Selective Syngas/H2 Production via Partial Oxidation of CH_4 Using (Ni, Co and Ni-Co)/ZrO_2-Al_2O_3 Catalysts: Influence of Calcination Temperature. *Processes* **2019**, *7*, 141. [CrossRef]
112. Li, Y.; Wang, J.; Ding, C.; Ma, L.; Xue, Y.; Guo, J.; Wang, S.; Meng, Y.; Zhang, K.; Liu, P. Effect of Cobalt Addition on the Structure and Properties of Ni-MCM-41 for the Partial Oxidation of Methane to Syngas. *RSC Adv.* **2019**, *9*, 25508–25517. [CrossRef] [PubMed]
113. Javed, A.H.; Shahzad, N.; Butt, F.A.; Khan, M.A.; Naeem, N.; Liaquat, R.; Khoja, A.H. Synthesis of Bimetallic Co-Ni/ZnO Nanoprisms (ZnO-NPr) for Hydrogen-Rich Syngas Production via Partial Oxidation of Methane. *J. Environ. Chem. Eng.* **2021**, *9*, 106887. [CrossRef]
114. Shooli, Z.S.; Izadbakhsh, A.; Sanati, A.M. Effect of Copper and Cerium on the Performance of Ni-SBA-16 in the Partial Oxidation of Methane. *Reac Kinet. Mech. Cat.* **2018**, *124*, 873–889. [CrossRef]
115. Ferreira, A.C.; Ferraria, A.M.; do Rego, A.M.B.; Gonçalves, A.P.; Girão, A.V.; Correia, R.; Gasche, T.A.; Branco, J.B. Partial Oxidation of Methane over Bimetallic Copper-Cerium Oxide Catalysts. *J. Mol. Catal. A Chem.* **2010**, *320*, 47–55. [CrossRef]
116. Emamdoust, A.; La Parola, V.; Pantaleo, G.; Testa, M.L.; Farjami Shayesteh, S.; Venezia, A.M. Partial Oxidation of Methane over SiO_2 Supported Ni and NiCe Catalysts. *J. Energy Chem.* **2020**, *47*, 1–9. [CrossRef]
117. Loktev, A.S.; Mukhin, I.E.; Bykov, M.A.; Sadovnikov, A.A.; Osipov, A.K.; Dedov, A.G. Novel High-Performance Catalysts for Partial Oxidation and Dry Reforming of Methane to Synthesis Gas. *Pet. Chem.* **2022**, *62*, 526–543. [CrossRef]
118. Gavrikov, A.V.; Loktev, A.S.; Ilyukhin, A.B.; Mukhin, I.E.; Bykov, M.A.; Vorobei, A.M.; Parenago, O.O.; Cherednichenko, K.A.; Sadovnikov, A.A.; Dedov, A.G. Partial Oxidation of Methane to Syngas over SmCoO3-Derived Catalysts: The Effect of the Supercritical Fluid Assisted Modification of the Perovskite Precursor. *Int. J. Hydrogen Energy* **2023**, *48*, 2998–3012. [CrossRef]
119. Wang, H.; Dai, H. Isovalent Substituted La-Gd-Cr Perovskite for the Cleaner Hydrogen Production during Partial Oxidation Methane in Catalytic Packed Bed. *Fuel* **2023**, *340*, 127457. [CrossRef]
120. Cui, Y.; Liu, Q.; Yao, Z.; Dou, B.; Shi, Y.; Sun, Y. A Comparative Study of Molybdenum Phosphide Catalyst for Partial Oxidation and Dry Reforming of Methane. *Int. J. Hydrogen Energy* **2019**, *44*, 11441–11447. [CrossRef]
121. Levikhin, A.A.; Boryaev, A.A. High-Temperature Reactor for Hydrogen Production by Partial Oxidation of Hydrocarbons. *Int. J. Hydrogen Energy* **2023**, *48*, 28187–28204. [CrossRef]
122. Khan, S.N.; Yang, Z.; Dong, W.; Zhao, M. Cost and Technology Readiness Level Assessment of Emerging Technologies, New Perspectives, and Future Research Directions in H_2 Production. *Sustain. Energy Fuels* **2022**, *6*, 4357–4374. [CrossRef]

123. Basini, L.E.; Guarinoni, A. Short Contact Time Catalytic Partial Oxidation (SCT-CPO) for Synthesis Gas Processes and Olefins Production. *Ind. Eng. Chem. Res.* **2013**, *52*, 17023–17037. [CrossRef]
124. Kale, G.R.; Doke, S.; Anjikar, A. Process Thermoneutral Point in Dry Autothermal Reforming for CO_2 Utilization. *J. CO2 Util.* **2017**, *18*, 318–325. [CrossRef]
125. Li, W.; Zhao, Z.; Ding, F.; Guo, X.; Wang, G. Syngas Production via Steam-CO_2 Dual Reforming of Methane over LA-Ni/ZrO_2 Catalyst Prepared by l -Arginine Ligand-Assisted Strategy: Enhanced Activity and Stability. *ACS Sustain. Chem. Eng.* **2015**, *3*, 3461–3476. [CrossRef]
126. Izquierdo, U.; Barrio, V.L.; Requies, J.; Cambra, J.F.; Güemez, M.B.; Arias, P.L. Tri-Reforming: A New Biogas Process for Synthesis Gas and Hydrogen Production. *Int. J. Hydrogen Energy* **2013**, *38*, 7623–7631. [CrossRef]
127. Chein, R.Y.; Hsu, W.H. Analysis of Syngas Production from Biogas via the Tri-Reforming Process. *Energies* **2018**, *11*, 1075. [CrossRef]
128. Mosinska, M.; Szynkowska, M.I.; Mierczynski, P. Oxy-Steam Reforming of Natural Gas on Ni Catalysts-A Minireview. *Catalysts* **2020**, *10*, 896. [CrossRef]
129. Griffiths, S.; Sovacool, B.K.; Kim, J.; Bazilian, M.; Uratani, J.M. Industrial Decarbonization via Hydrogen: A Critical and Systematic Review of Developments, Socio-Technical Systems and Policy Options. *Energy Res. Soc. Sci.* **2021**, *80*, 102208. [CrossRef]
130. Sepehri, S.; Rezaei, M.; Garbarino, G.; Busca, G. Facile Synthesis of a Mesoporous Alumina and Its Application as a Support of Ni-Based Autothermal Reforming Catalysts. *Int. J. Hydrogen Energy* **2016**, *41*, 3456–3464. [CrossRef]
131. Sepehri, S.; Rezaei, M.; Garbarino, G.; Busca, G. Preparation and Characterization of Mesoporous Nanocrystalline La-, Ce-, Zr-, Sr-Containing Ni-Al_2O_3 Methane Autothermal Reforming Catalysts. *Int. J. Hydrogen Energy* **2016**, *41*, 8855–8862. [CrossRef]
132. Sepehri, S.; Rezaei, M. Ce Promoting Effect on the Activity and Coke Formation of Ni Catalysts Supported on Mesoporous Nanocrystalline γ-Al_2O_3 in Autothermal Reforming of Methane. *Int. J. Hydrogen Energy* **2017**, *42*, 11130–11138. [CrossRef]
133. Matus, E.V.; Ismagilov, I.Z.; Yashnik, S.A.; Ushakov, V.A.; Prosvirin, I.P.; Kerzhentsev, M.A.; Ismagilov, Z.R. Hydrogen Production through Autothermal Reforming of CH_4: Efficiency and Action Mode of Noble (M = Pt, Pd) and Non-Noble (M = Re, Mo, Sn) Metal Additives in the Composition of Ni-M/$Ce_{0.5}Zr_{0.5}O_2$/Al_2O_3 Catalysts. *Int. J. Hydrogen Energy* **2020**, *45*, 33352–33369. [CrossRef]
134. Araújo, P.M.; da Costa, K.M.; Passos, F.B. Hydrogen Production from Methane Autothermal Reforming over CaTiO3, BaTiO3 and SrTiO3 Supported Nickel Catalysts. *Int. J. Hydrogen Energy* **2021**, *46*, 24107–24116. [CrossRef]
135. Tariq, R.; Maqbool, F.; Abbas, S.Z. Small-Scale Production of Hydrogen via Auto-Thermal Reforming in an Adiabatic Packed Bed Reactor: Parametric Study and Reactor's Optimization through Response Surface Methodology. *Comput. Chem. Eng.* **2021**, *145*, 107192. [CrossRef]
136. Murmura, M.A.; Diana, M.; Spera, R.; Annesini, M.C. Modeling of Autothermal Methane Steam Reforming: Comparison of Reactor Configurations. *Chem. Eng. Process. Process. Intensif.* **2016**, *109*, 125–135. [CrossRef]
137. Chen, B.; Wang, F. Numerical Simulation of Heat-Pipe and Folded Reformers for Efficient Hydrogen Production through Methane Autothermal Reforming. *Int. J. Energy Res.* **2020**, *44*, 10430–10441. [CrossRef]
138. Shahhosseini, H.R.; Saeidi, S.; Najari, S.; Gallucci, F. Comparison of Conventional and Spherical Reactor for the Industrial Auto-Thermal Reforming of Methane to Maximize Synthesis Gas and Minimize CO_2. *Int. J. Hydrogen Energy* **2017**, *42*, 19798–19809. [CrossRef]
139. Gul, H.; Arshad, M.Y.; Tahir, M.W. Production of H2 via Sorption Enhanced Auto-Thermal Reforming for Small Scale Applications-A Process Modeling and Machine Learning Study. *Int. J. Hydrogen Energy* **2023**, *48*, 12622–12635. [CrossRef]
140. Rau, F.; Herrmann, A.; Krause, H.; Fino, D.; Trimis, D. Production of Hydrogen by Autothermal Reforming of Biogas. *Energy Procedia* **2017**, *120*, 294–301. [CrossRef]
141. Rau, F.; Herrmann, A.; Krause, H.; Fino, D.; Trimis, D. Efficiency of a Pilot-Plant for the Autothermal Reforming of Biogas. *Int. J. Hydrogen Energy* **2019**, *44*, 19135–19140. [CrossRef]
142. Montenegro Camacho, Y.S.; Bensaid, S.; Piras, G.; Antonini, M.; Fino, D. Techno-Economic Analysis of Green Hydrogen Production from Biogas Autothermal Reforming. *Clean Technol. Environ. Policy* **2017**, *19*, 1437–1447. [CrossRef]
143. Kelling, R.; Eigenberger, G.; Nieken, U. Ceramic Counterflow Reactor for Autothermal Dry Reforming at High Temperatures. *Catal. Today* **2016**, *273*, 196–204. [CrossRef]
144. Akri, M.; Achak, O.; Granger, P.; Wang, S.; Batiot-Dupeyrat, C.; Chafik, T. Autothermal Reforming of Model Purified Biogas Using an Extruded Honeycomb Monolith: A New Catalyst Based on Nickel Incorporated Illite Clay Promoted with MgO. *J. Clean. Prod.* **2018**, *171*, 377–389. [CrossRef]
145. Dega, F.B.; Chamoumi, M.; Braidy, N.; Abatzoglou, N. Autothermal Dry Reforming of Methane with a Nickel Spinellized Catalyst Prepared from a Negative Value Metallurgical Residue. *Renew. Energy* **2019**, *138*, 1239–1249. [CrossRef]
146. Dega, F.B.; Abatzoglou, N. H 2 S Poisoning and Regeneration of a Nickel Spinellized Catalyst Prepared from Waste Metallurgical Residues, During Dry Autothermal Methane Reforming. *Catal. Lett.* **2019**, *149*, 1730–1742. [CrossRef]
147. Rosha, P.; Mohapatra, S.K.; Mahla, S.K.; Dhir, A. Hydrogen Enrichment of Biogas via Dry and Autothermal-Dry Reforming with Pure Nickel (Ni) Nanoparticle. *Energy* **2019**, *172*, 733–739. [CrossRef]
148. Khalighi, R.; Bahadoran, F.; Panjeshahi, M.H.; Zamaniyan, A.; Tahouni, N. High Catalytic Activity and Stability of X/$CoAl_2O_4$ (X = Ni, Co, Rh, Ru) Catalysts with No Observable Coke Formation Applied in the Autothermal Dry Reforming of Methane Lined on Cordierite Monolith Reactors. *Microporous Mesoporous Mater.* **2020**, *305*, 110371. [CrossRef]

149. Deng, G.; Zhang, G.; Zhu, X.; Guo, Q.; Liao, X.; Chen, X.; Li, K. Optimized Ni-Based Catalysts for Methane Reforming with O_2-Containing CO_2. *Appl. Catal. B* **2021**, *289*, 120033. [CrossRef]
150. Babakouhi, R.; Alavi, S.M.; Rezaei, M.; Akbari, E.; Varbar, M. Combined CO_2 Reforming and Partial Oxidation of Methane over Mesoporous Nanostructured Ni/M-Al_2O_3 Catalyst: Effect of Various Support Promoters and Nickel Loadings. *J. CO2 Util.* **2023**, *70*, 102427. [CrossRef]
151. Fan, D.; Gao, Y.; Liu, F.; Wei, T.; Ye, Z.; Ling, Y.; Chen, B.; Zhang, Y.; Ni, M.; Dong, D. Autothermal Reforming of Methane over an Integrated Solid Oxide Fuel Cell Reactor for Power and Syngas Co-Generation. *J. Power Sources* **2021**, *513*, 230536. [CrossRef]
152. Kumar, N.; Shojaee, M.; Spivey, J.J. Catalytic Bi-Reforming of Methane: From Greenhouse Gases to Syngas. *Curr. Opin. Chem. Eng.* **2015**, *9*, 8–15. [CrossRef]
153. Mohanty, U.S.; Ali, M.; Azhar, M.R.; Al-Yaseri, A.; Keshavarz, A.; Iglauer, S. Current Advances in Syngas (CO + H2) Production through Bi-Reforming of Methane Using Various Catalysts: A Review. *Int. J. Hydrogen Energy* **2021**, *46*, 32809–32845. [CrossRef]
154. Syed Muhammad Wajahat, U.H.; Ahmad, S.F.; Bamidele, V.A.; Bawadi, A. Syngas Production via Combined Dry and Steam Reforming Methane over Ni-Based Catalyst: A Review. *Mater. Res. Proc.* **2023**, *29*, 17–27. [CrossRef]
155. Jin, B.; Wang, K.; Yu, H.; He, X.; Liang, X. Engineering Oxygen Vacancy-Rich CeOx Overcoating onto Ni/Al_2O_3 by Atomic Layer Deposition for Bi-Reforming of Methane. *Chem. Eng. J.* **2023**, *459*, 141611. [CrossRef]
156. Panda, S.; Joshi, V.; Shrivastaw, V.; Das, S.; Poddar, M.K.; Bal, R.; Bordoloi, A. Enhanced Coke-Resistant Co-Modified Ni/Modified Alumina Catalyst for Bi-Reforming of Methane. *Catal. Sci. Technol.* **2023**, *13*, 4506–4516. [CrossRef]
157. Von Storch, H.; Becker-Hardt, S.; Sattler, C. (Solar) Mixed Reforming of Methane: Potential and Limits in Utilizing CO_2 as Feedstock for Syngas Production—A Thermodynamic Analysis. *Energies* **2018**, *11*, 2537. [CrossRef]
158. Matus, E.V.; Sukhova, O.B.; Ismagilov, I.Z.; Kerzhentsev, M.A.; Li, L.; Ismagilov, Z.R. Bi-Reforming of Methane: Thermodynamic Equilibrium Analysis and Selection of Preferable Reaction Conditions. *J. Phys. Conf. Ser.* **2021**, *1749*, 012023. [CrossRef]
159. Pham, X.H.; Ashik, U.P.M.; Hayashi, J.I.; Pérez Alonso, A.; Pla, D.; Gómez, M.; Pham Minh, D. Review on the Catalytic Tri-Reforming of Methane—Part II: Catalyst Development. *Appl. Catal. A Gen.* **2021**, *623*, 118286. [CrossRef]
160. Alli, R.D.; de Souza, P.A.L.; Mohamedali, M.; Virla, L.D.; Mahinpey, N. Tri-Reforming of Methane for Syngas Production Using Ni Catalysts: Current Status and Future Outlook. *Catal. Today* **2023**, *407*, 107–124. [CrossRef]
161. Soleimani, S.; Lehner, M. Tri-Reforming of Methane: Thermodynamics, Operating Conditions, Reactor Technology and Efficiency Evaluation—A Review. *Energies* **2022**, *15*, 7159. [CrossRef]
162. Kozonoe, C.E.; de Abreu, T.F.; de Brito Alves, R.M.; Schmal, M. Influence of the Material as Support for Nickel on the Product Selectivity of the Tri-Reforming of Methane. *Mater. Today Commun.* **2023**, *35*, 105732. [CrossRef]
163. Nascimento, J.P.; Bezerra, R.D.C.F.; Assaf, E.M.; Lucredio, A.F.; Araujo, R.S.; Saraiva, G.D.; Rodríguez-Castellón, E.; Rodríguez-Aguado, E.; Pinheiro, G.S.; Oliveira, A.C. Investigation of the Deactivation Behavior of MeMo/La_2O_3-Al_2O_3- and MeMo/Nb_2O_5 Supported Catalysts (Me = Pt, Ni, and Co) in Tri-Reforming of Methane. *Energy Fuels* **2023**, *37*, 3836–3853. [CrossRef]
164. Thyssen, V.V.; Lino, A.V.P.; Assaf, J.M.; Assaf, E.M. Syngas Production via Methane Tri-Reforming on Ni/La_2O_3–AAl_2O_3 Catalysts. *Braz. J. Chem. Eng.* **2023**. [CrossRef]
165. Bertoldi, J.; de Campos Roseno, K.T.; Schmal, M.; Lage, V.D.; Lenzi, G.G.; Brackmann, R. La_{1-x}(Ce, Sr)XNiO_3 Perovskite-Type Oxides as Catalyst Precursors to Syngas Production through Tri-Reforming of Methane. *Int. J. Hydrogen Energy* **2022**, *47*, 31279–31294. [CrossRef]
166. Jang, J.; Han, M. Tri-Reformer with O_2 Side-Stream Distribution for Syngas Production. *Int. J. Hydrogen Energy* **2022**, *47*, 9139–9155. [CrossRef]
167. Arab Aboosadi, Z.; Dehghanfard, E.; Abdosheikhi, M. Modeling of Methane Tri-Reforming Slurry Bubble Column Reactor via Differential Evolution Optimization Method to Produce Syngas. *Int. J. Chem. React. Eng.* **2022**, *20*, 911–928. [CrossRef]
168. Osat, M.; Shojaati, F.; Hafizi, A. A Multi-Objective Optimization of Three Conflicting Criteria in a Methane Tri-Reforming Reactor. *Int. J. Hydrogen Energy* **2023**, *48*, 6275–6287. [CrossRef]
169. Soltanimehr, S.; Rahimpour, M.R.; Shariati, A. Development of a Green Process Based on a Novel Tri-Reforming Reactor to Produce Syngas for Methanol Synthesis: Process Design, Modeling and Multi Objective Optimization. *J. Clean. Prod.* **2023**, *418*, 138167. [CrossRef]
170. McConnachie, M.; Konarova, M.; Smart, S. Literature Review of the Catalytic Pyrolysis of Methane for Hydrogen and Carbon Production. *Int. J. Hydrogen Energy* **2023**, *48*, 25660–25682. [CrossRef]
171. Muradov, N.Z.; Veziroğlu, T.N. From Hydrocarbon to Hydrogen-Carbon to Hydrogen Economy. *Int. J. Hydrogen Energy* **2005**, *30*, 225–237. [CrossRef]
172. Msheik, M.; Rodat, S.; Abanades, S. Methane Cracking for Hydrogen Production: A Review of Catalytic and Molten Media Pyrolysis. *Energies* **2021**, *14*, 3107. [CrossRef]
173. Korányi, T.I.; Németh, M.; Beck, A.; Horváth, A. Recent Advances in Methane Pyrolysis: Turquoise Hydrogen with Solid Carbon Production. *Energies* **2022**, *15*, 6342. [CrossRef]
174. Kang, D.; Rahimi, N.; Gordon, M.J.; Metiu, H.; McFarland, E.W. Catalytic Methane Pyrolysis in Molten $MnCl_2$-KCl. *Appl. Catal. B* **2019**, *254*, 659–666. [CrossRef]
175. Hu, X.; Hu, Y.; Xu, Q.; Wang, X.; Li, G.; Cheng, H.; Zou, X.; Lu, X. Molten Salt-Promoted Ni–Fe/Al_2O_3 Catalyst for Methane Decomposition. *Int. J. Hydrogen Energy* **2020**, *45*, 4244–4253. [CrossRef]

176. Boo, J.; Ko, E.H.; Park, N.K.; Ryu, C.; Kim, Y.H.; Park, J.; Kang, D. Methane Pyrolysis in Molten Potassium Chloride: An Experimental and Economic Analysis. *Energies* **2021**, *14*, 8182. [CrossRef]
177. Kazemi, S.; Alavi, S.M.; Rezaei, M.; Akbari, E. Fabrication and Evaluation of the Mn-Promoted Ni/$FeAl_2O_4$ Catalysts in the Thermocatalytic Decomposition of Methane: Impact of Various Promoters. *Fuel* **2023**, *342*, 127797. [CrossRef]
178. Miccio, F. On the Integration between Fluidized Bed and Stirling Engine for Micro-Generation. *Appl. Therm. Eng.* **2013**, *52*, 46–53. [CrossRef]
179. Reshetenko, T.V.; Avdeeva, L.B.; Ismagilov, Z.R.; Chuvilin, A.L.; Ushakov, V.A. Carbon Capacious Ni-Cu-Al_2O_3 Catalysts for High-Temperature Methane Decomposition. *Appl. Catal. A Gen.* **2003**, *247*, 51–63. [CrossRef]
180. Ammendola, P.; Chirone, R.; Lisi, L.; Ruoppolo, G.; Russo, G. Copper Catalysts for H2 Production via CH_4 Decomposition. *J. Mol. Catal. A Chem.* **2007**, *266*, 31–39. [CrossRef]
181. Kunii, D. *Levenspiel Octave Fluidization Engineering-Chapter 3: Fluidization and Mapping of Regimes*; Butterworth-Heinemann: Newton, MA, USA, 1991; ISBN 978-0-08-050664-7.
182. Ammendola, P.; Chirone, R.; Ruoppolo, G.; Russo, G. Regeneration Strategies of Deactivated Catalysts for Thermo-Catalytic Decomposition Process in a Fluidized Bed Reactor. *Combust. Sci. Technol.* **2008**, *180*, 869–882. [CrossRef]
183. European Commission, Directorate-General for Internal Market, Industry, Entrepreneurship and SMEs. *European Commission Proposal for a REGULATION OF THE EUROPEAN PARLIAMENT AND OF THE COUNCIL a Framework for Ensuring a Secure and Sustainable Supply of Critical Raw and Amending Regulations (EU) 168/2013, (EU) 2018/858, 2018/1724 and (EU) 2019/1020*; European Commission, Directorate-General for Internal Market, Industry, Entrepreneurship and SMEs: Brussels, Belgium, 2023.
184. Bahman, N.; Al-Khalifa, M.; Al Baharna, S.; Abdulmohsen, Z.; Khan, E. Review of Carbon Capture and Storage Technologies in Selected Industries: Potentials and Challenges. *Rev. Environ. Sci. Biotechnol.* **2023**, *22*, 451–470. [CrossRef]
185. Steinberg, M. Fossil Fuel Decarbonization Technology for Mitigating Global Warming. *Int. J. Hydrogen Energy* **1999**, *24*, 771–777. [CrossRef]
186. Shamsi, M.; Moghaddas, S.; Naeiji, E.; Farokhi, S. Techno-Economic, Energy, Exergy, and Environmental Comparison of Hydrogen Production from Natural Gas, Biogas, and Their Combination as Feedstock. *Arab. J. Sci. Eng.* **2023**, *48*, 8971–8987. [CrossRef]
187. Szima, S.; Cormos, C.C. Techno—Economic Assessment of Flexible Decarbonized Hydrogen and Power Co-Production Based on Natural Gas Dry Reforming. *Int. J. Hydrogen Energy* **2019**, *44*, 31712–31723. [CrossRef]
188. Lee, B.; Kim, H.; Lee, H.; Byun, M.; Won, W.; Lim, H. Technical and Economic Feasibility under Uncertainty for Methane Dry Reforming of Coke Oven Gas as Simultaneous H_2 Production and CO_2 Utilization. *Renew. Sustain. Energy Rev.* **2020**, *133*, 110056. [CrossRef]
189. Farkad Alkhani, A. *Catalytic Dry Reforming of Methane: Paving the Road to a Carbon Neutral Industrial Scale Blue Hydrogen Production Process Technology via Monolithic Catalyst-Based Reformer Bolstered by a Techno-Economic Assessment*; Columbia University: New York, NY, USA, 2022.
190. Kumar, R.; Kumar, A.; Pal, A. An Overview of Conventional and Non-Conventional Hydrogen Production Methods. *Mater. Today Proc.* **2020**, *46*, 5353–5359. [CrossRef]
191. Sánchez-Bastardo, N.; Schlögl, R.; Ruland, H. Methane Pyrolysis for CO_2-Free H_2 Production: A Green Process to Overcome Renewable Energies Unsteadiness. *Chem. Ing. Tech.* **2020**, *92*, 1596–1609. [CrossRef]
192. Cheon, S.; Byun, M.; Lim, D.; Lee, H.; Lim, H. Parametric Study for Thermal and Catalytic Methane Pyrolysis for Hydrogen Production: Techno-Economic and Scenario Analysis. *Energies* **2021**, *14*, 6102. [CrossRef]
193. Li, D.; Xu, R.; Gu, Z.; Zhu, X.; Qing, S.; Li, K. Chemical-Looping Conversion of Methane: A Review. *Energy Technol.* **2020**, *8*, 1900925. [CrossRef]
194. Mantripragada, H.C.; Veser, G. Hydrogen Production via Chemical Looping Dry Reforming of Methane: Process Modeling and Systems Analysis. *AIChE J.* **2022**, *68*, e17612. [CrossRef]
195. Ugwu, A.; Zaabout, A.; Amini, S. An Advancement in CO_2 Utilization through Novel Gas Switching Dry Reforming. *Int. J. Greenh. Gas Control* **2019**, *90*, 102791. [CrossRef]
196. Hu, J.; Galvita, V.V.; Poelman, H.; Marin, G.B. Advanced Chemical Looping Materials for CO_2 Utilization: A Review. *Materials* **2018**, *11*, 1187. [CrossRef] [PubMed]
197. Yu, Z.; Yang, Y.; Yang, S.; Zhang, Q.; Zhao, J.; Fang, Y.; Hao, X.; Guan, G. Iron-Based Oxygen Carriers in Chemical Looping Conversions: A Review. *Carbon. Resour. Convers.* **2019**, *2*, 23–34. [CrossRef]
198. Chuayboon, S.; Abanades, S.; Rodat, S. Stepwise Solar Methane Reforming and Water-Splitting via Lattice Oxygen Transfer in Iron and Cerium Oxides. *Energy Technol.* **2020**, *8*, 1900415. [CrossRef]
199. Tang, M.; Xu, L.; Fan, M. Progress in Oxygen Carrier Development of Methane-Based Chemical-Looping Reforming: A Review. *Appl. Energy* **2015**, *151*, 143–156. [CrossRef]
200. Huang, Z.; He, F.; Chen, D.; Zhao, K.; Wei, G.; Zheng, A.; Zhao, Z.; Li, H. Investigation on Reactivity of Iron Nickel Oxides in Chemical Looping Dry Reforming. *Energy* **2016**, *116*, 53–63. [CrossRef]
201. Sastre, D.; Galván, C.Á.; Pizarro, P.; Coronado, J.M. Enhanced Performance of CH_4 Dry Reforming over $La_{0.9}Sr_{0.1}FeO_3$/YSZ under Chemical Looping Conditions. *Fuel* **2022**, *309*, 122122. [CrossRef]
202. Forutan, H.R.; Karimi, E.; Hafizi, A.; Rahimpour, M.R.; Keshavarz, P. Expert Representation Chemical Looping Reforming: A Comparative Study of Fe, Mn, Co and Cu as Oxygen Carriers Supported on Al_2O_3. *J. Ind. Eng. Chem.* **2015**, *21*, 900–911. [CrossRef]

203. Löfberg, A.; Guerrero-Caballero, J.; Kane, T.; Rubbens, A.; Jalowiecki-Duhamel, L. Ni/CeO_2 Based Catalysts as Oxygen Vectors for the Chemical Looping Dry Reforming of Methane for Syngas Production. *Appl. Catal. B* **2017**, *212*, 159–174. [CrossRef]
204. Guerrero-Caballero, J.; Kane, T.; Haidar, N.; Jalowiecki-Duhamel, L.; Löfberg, A. Ni, Co, Fe Supported on Ceria and Zr Doped Ceria as Oxygen Carriers for Chemical Looping Dry Reforming of Methane. *Catal. Today* **2019**, *333*, 251–258. [CrossRef]
205. Noh, Y.G.; Lee, Y.J.; Kim, J.; Kim, Y.K.; Ha, J.S.; Kalanur, S.S.; Seo, H. Enhanced Efficiency in CO_2-Free Hydrogen Production from Methane in a Molten Liquid Alloy Bubble Column Reactor with Zirconia Beads. *Chem. Eng. J.* **2021**, *428*, 131095. [CrossRef]
206. Miccio, F.; Papa, E.; Murri, A.N.; Landi, E.; Medri, V.; Vaccari, A. Fluidized Bed Gasification of Biomass Char by Chemical Looping. *Chem. Eng. Trans.* **2021**, *86*, 769–774. [CrossRef]
207. Kang, D.; Lee, M.; Lim, H.S.; Lee, J.W. Chemical Looping Partial Oxidation of Methane with CO_2 Utilization on the Ceria-Enhanced Mesoporous Fe_2O_3 Oxygen Carrier. *Fuel* **2018**, *215*, 787–798. [CrossRef]
208. García-García, F.R.; Metcalfe, I.S. Chemical Looping Dry Reforming of Methane Using Mixed Oxides of Iron and Cerium: Operation Window. *Catal. Commun.* **2021**, *160*, 106356. [CrossRef]
209. Cao, Z.; Zhu, X.; Li, K.; Wei, Y.; He, F.; Wang, H. Moderate-Temperature Chemical Looping Splitting of CO_2 and H_2O for Syngas Generation. *Chem. Eng. J.* **2020**, *397*, 125393. [CrossRef]
210. Haxel, G.B.; Hedrick, J.B.; Orris, G.J. Rare Earth Elements—Critical Resources for High Technology. Available online: https://pubs.usgs.gov/fs/2002/fs087-02/ (accessed on 25 May 2022).
211. Otsuka, K.; Ushiyama, T.; Yamanaka, I. Partial Oxidation of Methane Using the Redox of Cerium Oxide. *Chem. Lett.* **1993**, *22*, 1517–1520. [CrossRef]
212. Schmitt, R.; Nenning, A.; Kraynis, O.; Korobko, R.; Frenkel, A.I.; Lubomirsky, I.; Haile, S.M.; Rupp, J.L.M. A Review of Defect Structure and Chemistry in Ceria and Its Solid Solutions. *Chem. Soc. Rev.* **2020**, *49*, 554–592. [CrossRef]
213. Li, P.; Chen, X.; Li, Y.; Schwank, J.W. A Review on Oxygen Storage Capacity of CeO_2-Based Materials: Influence Factors, Measurement Techniques, and Applications in Reactions Related to Catalytic Automotive Emissions Control. *Catal. Today* **2019**, *327*, 90–115. [CrossRef]
214. Nair, M.M.; Abanades, S. Tailoring Hybrid Nonstoichiometric Ceria Redox Cycle for Combined Solar Methane Reforming and Thermochemical Conversion of H_2O/CO_2. *Energy Fuels* **2016**, *30*, 6050–6058. [CrossRef]
215. Montini, T.; Melchionna, M.; Monai, M.; Fornasiero, P. Fundamentals and Catalytic Applications of CeO_2-Based Materials. *Chem. Rev.* **2016**, *116*, 5987–6041. [CrossRef]
216. Rotaru, C.G.; Postole, G.; Florea, M.; Matei-Rutkovska, F.; Pârvulescu, V.I.; Gelin, P. Dry Reforming of Methane on Ceria Prepared by Modified Precipitation Route. *Appl. Catal. A Gen.* **2015**, *494*, 29–40. [CrossRef]
217. Miccio, F.; Landi, E.; Murri, A.N.; Minelli, M.; Doghieri, F.; Storione, A. Fluidized Bed Reforming of Methane by Chemical Looping with Cerium Oxide Oxygen Carriers. *Chem. Eng. Res. Des.* **2023**, *191*, 568–577. [CrossRef]
218. Ackermann, S.; Scheffe, J.R.; Steinfeld, A. Diffusion of Oxygen in Ceria at Elevated Temperatures and Its Application to H_2O/CO_2 Splitting Thermochemical Redox Cycles. *J. Phys. Chem. C* **2014**, *118*, 5216–5225. [CrossRef]
219. Teh, L.P.; Setiabudi, H.D.; Timmiati, S.N.; Aziz, M.A.A.; Annuar, N.H.R.; Ruslan, N.N. Recent Progress in Ceria-Based Catalysts for the Dry Reforming of Methane: A Review. *Chem. Eng. Sci.* **2021**, *242*, 116606. [CrossRef]
220. Ramírez-Cabrera, E.; Atkinson, A.; Chadwick, D. Reactivity of Ceria, Gd- and Nb-Doped Ceria to Methane. *Appl. Catal. B* **2002**, *36*, 193–206. [CrossRef]
221. Jeong, H.H.; Kwak, J.H.; Han, G.Y.; Yoon, K.J. Stepwise Production of Syngas and Hydrogen through Methane Reforming and Water Splitting by Using a Cerium Oxide Redox System. *Int. J. Hydrogen Energy* **2011**, *36*, 15221–15230. [CrossRef]
222. Matei-Rutkovska, F.; Postole, G.; Rotaru, C.G.; Florea, M.; Pârvulescu, V.I.; Gelin, P. Synthesis of Ceria Nanopowders by Microwave-Assisted Hydrothermal Method for Dry Reforming of Methane. *Int. J. Hydrogen Energy* **2016**, *41*, 2512–2525. [CrossRef]
223. Warren, K.J.; Carrillo, R.J.; Greek, B.; Hill, C.M.; Scheffe, J.R. Solar Reactor Demonstration of Efficient and Selective Syngas Production via Chemical-Looping Dry Reforming of Methane over Ceria. *Energy Technol.* **2020**, *8*, 1–13. [CrossRef]
224. Chuayboon, S.; Abanades, S.; Rodat, S. Solar Chemical Looping Reforming of Methane Combined with Isothermal H_2O/CO_2 Splitting Using Ceria Oxygen Carrier for Syngas Production. *J. Energy Chem.* **2020**, *41*, 60–72. [CrossRef]
225. Krenzke, P.T.; Davidson, J.H. Thermodynamic Analysis of Syngas Production via the Solar Thermochemical Cerium Oxide Redox Cycle with Methane-Driven Reduction. *Energy Fuels* **2014**, *28*, 4088–4095. [CrossRef]
226. Storione, A.; Minelli, M.; Doghieri, F.; Landi, E.; Miccio, F. Thermodynamic Study on the Feasibility of a New Combined Chemical Looping Process for Syngas Production. *Chem. Eng. Trans.* **2021**, *86*, 1267–1272. [CrossRef]
227. Warren, K.J.; Scheffe, J.R. Role of Surface Oxygen Vacancy Concentration on the Dissociation of Methane over Nonstoichiometric Ceria. *J. Phys. Chem. C* **2019**, *123*, 13208–13218. [CrossRef]
228. Ackermann, S.; Sauvin, L.; Castiglioni, R.; Rupp, J.L.M.; Scheffe, J.R.; Steinfeld, A. Kinetics of CO_2 Reduction over Nonstoichiometric Ceria. *J. Phys. Chem. C* **2015**, *119*, 16452–16461. [CrossRef] [PubMed]
229. Welte, M.; Warren, K.; Scheffe, J.R.; Steinfeld, A. Combined Ceria Reduction and Methane Reforming in a Solar-Driven Particle-Transport Reactor. *Ind. Eng. Chem. Res.* **2017**, *56*, 10300–10308. [CrossRef]
230. Diao, Y.; Wang, H.; Chen, B.; Zhang, X.; Shi, C. Modulating Morphology and Textural Properties of Al_2O_3 for Supported Ni Catalysts toward Plasma-Assisted Dry Reforming of Methane. *Appl. Catal. B* **2023**, *330*, 122573. [CrossRef]

231. Zhang, M.; Gao, Y.; Mao, Y.; Wang, W.; Sun, J.; Song, Z.; Sun, J.; Zhao, X. Enhanced Dry Reforming of Methane by Microwave-Mediated Confined Catalysis over Ni-La/AC Catalyst. *Chem. Eng. J.* **2023**, *451*, 138616. [CrossRef]
232. Mei, D.; Sun, M.; Liu, S.; Zhang, P.; Fang, Z.; Tu, X. Plasma-Enabled Catalytic Dry Reforming of CH_4 into Syngas, Hydrocarbons and Oxygenates: Insight into the Active Metals of γ-Al_2O_3 Supported Catalysts. *J. CO2 Util.* **2023**, *67*, 102307. [CrossRef]
233. Kim, H.J.; Chun, Y.N. Conversion of Biogas to Renewable Energy by Microwave Reforming. *Energies* **2020**, *13*, 4093. [CrossRef]
234. Gray, J.T.; Che, F.; McEwen, J.S.; Ha, S. Field-Assisted Suppression of Coke in the Methane Steam Reforming Reaction. *Appl. Catal. B* **2020**, *260*, 118132. [CrossRef]
235. Zehetner, E.; Schöny, G.; Fuchs, J.; Pröll, T.; Hofbauer, H. Fluid-Dynamic Study on a Multistage Fluidized Bed Column for Continuous CO_2 Capture via Temperature Swing Adsorption. *Powder Technol.* **2017**, *316*, 528–534. [CrossRef]
236. Chen, Z.; Hou, Y.; Yang, Y.; Cai, D.; Song, W.; Wang, N.; Qian, W. A Multi-Stage Fluidized Bed Strategy for the Enhanced Conversion of Methanol into Aromatics. *Chem. Eng. Sci.* **2019**, *204*, 1–8. [CrossRef]
237. Wang, S.; Yan, L.; Zhao, F.; Lu, H.; Sun, L.; Zhang, Q. Numerical Simulation of Hydrogen Production via Chemical Looping Reforming in Interconnected Fluidized Bed Reactor. *Ind. Eng. Chem. Res.* **2014**, *53*, 4182–4191. [CrossRef]
238. Durán, P.; Sanz-Martínez, A.; Soler, J.; Menéndez, M.; Herguido, J. Pure Hydrogen from Biogas: Intensified Methane Dry Reforming in a Two-Zone Fluidized Bed Reactor Using Permselective Membranes. *Chem. Eng. J.* **2019**, *370*, 772–781. [CrossRef]
239. Zambrano, D.; Soler, J.; Herguido, J.; Menéndez, M. Conventional and Improved Fluidized Bed Reactors for Dry Reforming of Methane: Mathematical Models. *Chem. Eng. J.* **2020**, *393*, 124775. [CrossRef]
240. Driessen, R.T.; Bos, M.J.; Brilman, D.W.F. A Multistage Fluidized Bed for the Deep Removal of Sour Gases: Proof of Concept and Tray Efficiencies. *Ind. Eng. Chem. Res.* **2018**, *57*, 3866–3875. [CrossRef]
241. Ko, K.J.; Kim, H.; Cho, Y.H.; Lee, H.; Kim, K.M.; Lee, C.H. Overview of Carbon Monoxide Adsorption Performance of Pristine and Modified Adsorbents. *J. Chem. Eng. Data* **2022**, *67*, 1599–1616. [CrossRef]
242. Baker, R.W.; Low, B.T. Gas Separation Membrane Materials: A Perspective. *Macromolecules* **2014**, *47*, 6999–7013. [CrossRef]
243. Sanders, D.F.; Smith, Z.P.; Guo, R.; Robeson, L.M.; McGrath, J.E.; Paul, D.R.; Freeman, B.D. Energy-Efficient Polymeric Gas Separation Membranes for a Sustainable Future: A Review. *Polymer* **2013**, *54*, 4729–4761. [CrossRef]
244. Bernardo, G.; Araújo, T.; da Silva Lopes, T.; Sousa, J.; Mendes, A. Recent Advances in Membrane Technologies for Hydrogen Purification. *Int. J. Hydrogen Energy* **2020**, *45*, 7313–7338. [CrossRef]
245. Teplyakov, V. Polymeric Membranes for Hydrogen Separation/Purification. In *Current Trends and Future Developments on (Bio-) Membranes: New Perspectives on Hydrogen Production, Separation, and Utilization*; Elsevier: Amsterdam, The Netherlands, 2020; pp. 281–304, ISBN 9780128173848.
246. Amosova, O.L.; Malykh, O.V.; Teplyakov, V.V. Integrated Membrane/PSA Systems for Hydrogen Recovery from Gas Mixtures. *Desalination Water Treat.* **2010**, *14*, 119–126. [CrossRef]
247. Adhikari, S.; Fernando, S. Hydrogen Membrane Separation Techniques. *Ind. Eng. Chem. Res.* **2006**, *45*, 875–881. [CrossRef]
248. Wang, D.; Flanagan, T.B.; Shanahan, K.L. Permeation of Hydrogen through Pre-Oxidized Pd Membranes in the Presence and Absence of CO. *J. Alloys Compd.* **2004**, *372*, 158–164. [CrossRef]
249. Catalano, J.; Giacinti Baschetti, M.; Sarti, G.C. Hydrogen Permeation in Palladium-Based Membranes in the Presence of Carbon Monoxide. *J. Memb. Sci.* **2010**, *362*, 221–233. [CrossRef]
250. Koutsonikolas, D.E.; Pantoleontos, G.; Karagiannakis, G.; Konstandopoulos, A.G. Development of H2 Selective Silica Membranes: Performance Evaluation through Single Gas Permeation and Gas Separation Tests. *Sep. Purif. Technol.* **2021**, *264*, 118432. [CrossRef]
251. Mercadelli, E.; Gondolini, A.; Ardit, M.; Cruciani, G.; Melandri, C.; Escolástico, S.; Serra, J.M.; Sanson, A. Chemical and Mechanical Stability of BCZY-GDC Membranes for Hydrogen Separation. *Sep. Purif. Technol.* **2022**, *289*, 120795. [CrossRef]
252. Raganati, F.; Miccio, F.; Ammendola, P. Adsorption of Carbon Dioxide for Post-Combustion Capture: A Review. *Energy Fuels* **2021**, *35*, 12845–12868. [CrossRef]
253. Iarikov, D.D.; Ted Oyama, S. Chapter 5—Review of CO_2/CH_4 Separation Membranes. In *Membrane Science and Technology*; Oyama, S.T., Stagg-Williams, S.M., Eds.; Elsevier: Amsterdam, The Netherlands, 2011; Volume 14, pp. 91–115, ISBN 9780444537287.
254. Minelli, M.; Doghieri, F.; Miccio, F.; Landi, E.; Medri, V. New Hybrid Unit Operation for Gas Separation Membranes Application. *Chem. Eng. Trans.* **2019**, *74*, 925–930. [CrossRef]
255. Li, B.; Kado, S.; Mukainakano, Y.; Nurunnabi, M.; Miyao, T.; Naito, S.; Kunimori, K.; Tomishige, K. Temperature Profile of Catalyst Bed during Oxidative Steam Reforming of Methane over Pt-Ni Bimetallic Catalysts. *Appl. Catal. A Gen.* **2006**, *304*, 62–71. [CrossRef]
256. Karim, A.; Bravo, J.; Datye, A. Nonisothermality in Packed Bed Reactors for Steam Reforming of Methanol. *Appl. Catal. A Gen.* **2005**, *282*, 101–109. [CrossRef]
257. Wesenberg, M.H.; Svendsen, H.F. Mass and Heat Transfer Limitations in a Heterogeneous Model of a Gas-Heated Steam Reformer. *Ind. Eng. Chem. Res.* **2007**, *46*, 667–676. [CrossRef]
258. Al-Otaibi, F.; Xiao, H.; Berrouk, A.S.; Polychronopoulou, K. Numerical Study of Dry Reforming of Methane in Packed and Fluidized Beds: Effects of Key Operating Parameters. *ChemEngineering* **2023**, *7*, 57. [CrossRef]
259. Han, Z.; Shao, Y.; Zhong, W. Experimental and Numerical Study on Characteristics and Mechanism of Particles Attrition in Fluidized Bed. *Powder Technol.* **2023**, *427*, 118444. [CrossRef]

260. Zhou, Y.; Wang, T.; Zhu, J. Development of Gas-Solid Fluidization: Particulate and Aggregative. *Powder Technol.* **2023**, *421*, 118420. [CrossRef]
261. Côté, A.S.; Delgass, W.N.; Ramkrishna, D. Spatially Patterned Catalytic Reactors. Feasibility Issues. *Chem. Eng. Sci.* **2001**, *56*, 1011–1019. [CrossRef]
262. Mcbride, K.; Turek, T.; Güttel, R. Direct Dimethyl Ether Synthesis by Spatial Patterned Catalyst Arrangement: A Modeling and Simulation Study. *AIChE J.* **2012**, *58*, 3468–3473. [CrossRef]
263. Pajak, M.; Mozdzierz, M.; Chalusiak, M.; Kimijima, S.; Szmyd, J.S.; Brus, G. A Numerical Analysis of Heat and Mass Transfer Processes in a Macro-Patterned Methane/Steam Reforming Reactor. *Int. J. Hydrogen Energy* **2018**, *43*, 20474–20487. [CrossRef]
264. Cherif, A.; Nebbali, R.; Lee, C.J. Numerical Analysis of Steam Methane Reforming over a Novel Multi-Concentric Rings Ni/Al_2O_3 Catalyst Pattern. *Int. J. Energy Res.* **2021**, *45*, 18722–18734. [CrossRef]
265. Pajak, M.; Buchaniec, S.; Kimijima, S.; Szmyd, J.S.; Brus, G. A Multiobjective Optimization of a Catalyst Distribution in a Methane/Steam Reforming Reactor Using a Genetic Algorithm. *Int. J. Hydrogen Energy* **2021**, *46*, 20183–20197. [CrossRef]
266. Pajak, M.; Brus, G.; Kimijima, S.; Szmyd, J.S. Enhancing Hydrogen Production from Biogas through Catalyst Rearrangements. *Energies* **2023**, *16*, 4058. [CrossRef]
267. Lee, J.; Kim, B.; Han, M. Spatially Patterned Catalytic Reactor for Steam-CO_2 Reforming of Methane. *Ind. Eng. Chem. Res.* **2019**, *58*, 18731–18741. [CrossRef]
268. Wu, Z.; Guo, Z.; Yang, J.; Wang, Q. Effect of Diameter Distribution of Particles on Methane Steam Reforming in Multi-Channel Grille-Sphere Composite Packed Bed. *Energy Convers. Manag.* **2022**, *265*, 115764. [CrossRef]
269. Karpilov, I.; Pashchenko, D. Steam Methane Reforming over a Preheated Packed Bed: Heat and Mass Transfer in a Transient Process. *Therm. Sci. Eng. Prog.* **2023**, *42*, 101868. [CrossRef]
270. Cherif, A.; Nebbali, R.; Sheffield, J.W.; Doner, N.; Sen, F. Numerical Investigation of Hydrogen Production via Autothermal Reforming of Steam and Methane over Ni/Al_2O_3 and Pt/Al_2O_3 Patterned Catalytic Layers. *Int. J. Hydrogen Energy* **2021**, *46*, 37521–37532. [CrossRef]
271. Cherif, A.; Nebbali, R.; Sen, F.; Sheffield, J.W.; Doner, N.; Nasseri, L. Modeling and Simulation of Steam Methane Reforming and Methane Combustion over Continuous and Segmented Catalyst Beds in Autothermal Reactor. *Int. J. Hydrogen Energy* **2022**, *47*, 9127–9138. [CrossRef]
272. Cherif, A.; Lee, J.S.; Nebbali, R.; Lee, C.J. Novel Design and Multi-Objective Optimization of Autothermal Steam Methane Reformer to Enhance Hydrogen Production and Thermal Matching. *Appl. Therm. Eng.* **2022**, *217*, 119140. [CrossRef]
273. Mundhwa, M.; Thurgood, C.P. Improved Performance of a Catalytic Plate Reactor Coated with Distributed Layers of Reforming and Combustion Catalysts for Hydrogen Production. *React. Chem. Eng.* **2018**, *3*, 487–514. [CrossRef]
274. Lee, S.; Lim, H. Utilization of CO_2 Arising from Methane Steam Reforming Reaction: Use of CO_2 Membrane and Heterotic Reactors. *J. Ind. Eng. Chem.* **2020**, *91*, 201–212. [CrossRef]
275. Cherif, A.; Nebbali, R.; Lee, C.J. Design and Multiobjective Optimization of Membrane Steam Methane Reformer: A Computational Fluid Dynamic Analysis. *Int. J. Energy Res.* **2022**, *46*, 8700–8715. [CrossRef]